Modeling and characterizing bi-directional airflow in natural ventilation

by

Qin Zhang

B.S., Building Technology. B.A., Economics.
Tsinghua University, 2014

Submitted to the Department of Architecture
in Partial Fulfillment of the Requirements for the Degree of

Master of Science in Building Technology
at the
Massachusetts Institute of Technology

June 2016

Signature of Author: Signature redacted
Department of Architecture
May 13, 2016

Certified by: Signature redacted
Leon R. Glicksman
Professor of Building Technology and Mechanical Engineering
Thesis Supervisor

Accepted by: Signature redacted
Takehiko Nagakura
Associate Professor of Design and Computation
Chair of the Department Committee for Graduate Student

[this page intentionally left blank]

Modeling and characterizing bi-directional airflow in natural ventilation

by

Qin Zhang

Submitted to the Department of Architecture on May 13, 2016
in Partial Fulfillment of the Requirements for the Degree of

Master of Science in Building Technology

ABSTRACT

Bi-directional airflow in natural ventilation is an essential but not-well-understood scenario due to the complexity of airflow patterns as well as the strong coupling effect between temperature and ventilation. Neglecting bi-directional natural ventilation will result in problematic solutions and inaccuracy in estimation of ventilation performance. This work is focused on filling the knowledge gap by understanding the bi-directional airflow using computational fluid dynamics (CFD). Two important scenarios are simulated and analyzed: 1. Two-zone model with pure buoyancy forces, 2. Multi-zone model with combined wind and buoyancy forces. In the 1st model, a new concept of "local discharge coefficient" is proposed for its consistency under different boundary conditions. The influence of radiative heat transfer on simulation accuracy and ventilation performance is also investigated. In the 2nd model, the transient behaviors of airflow and the dynamics of wind and buoyant forces are analyzed and characterized.

A new physical model is proposed based on simplified assumptions and nondimensionalization. This model is able to predicting the transient behavior of multi-zonal ventilation that involves bi-directional airflow patterns. The result of this study is to be integrated in CoolVent, the software designed by Building Technology Lab.

Thesis Supervisor: Leon. R. Glicksman

Title: Professor of Building Technology and Mechanical Engineering

Thesis Supervisor:
Leon R. Glicksman, Professor of Building Technology and Mechanical Engineering, MIT

[this page intentionally left blank]

ACKNOWLEDGEMENTS

First of all, I wish to express my heartfelt gratitude to my academic and research advisor, Prof. Leon R. Glicksman. You inspire, encourage, and motivate me to explore the profound field of "thermo-fluids in buildings" in this open and creative Building Technology Lab. It's a privilege for me to have the opportunity to work with and learn from you.

I also wish to give my salute to all the faculties, staffs and students in the Building Technology Program. Especially, Professor Leslie K. Norford, for your generous advice and valuable instruction on funding problems, research progress and teaching assistantship; Departmental Administrator Kathleen Ross, for your attentive help and assistance for me.

I want to thank my undergraduate advisor, Professor Xudong Yang, BT alumni and now deputy chair of Building Technology Program in Tsinghua University, for your continuous support and disinterested advice about my life goals and academic pursuit over the past four years.

I also want to thank my friend, Alonso Dominguez Espinosa, who has always been giving me helpful research advising and sincere life guidance. I also want to thank my cheerful BT folks, Alpha Arsano, Jamie Voros, David Blum, Carlos Cerezo, Tianyi Chen, and Lup Wai Chew. Your friendship made me feel warm and supported through all the up and downs in the two years.

I also like to thank Jordan Alexander Goldstein for your unconditional support throughout the whole process of writing this thesis. Without your unwavering encouragement, this accomplishment would not have been made possible.

I would also like to give my highest respect and gratitude to my beloved parents. Without your consistent support, unconditional trust and love, I would not have been able to finish the challenging two years at MIT. I feel blessed to have such wonderful parents who have always been there throughout all the tantrums, the milestones, and the tears in the past two years!

BIOGRAPHIC NOTE

I graduated from Tsinghua University with a *B.S. in Building Technology with honors* and *B.A in Economics* in July 2014, where I was exposed to comprehensive scopes of thermos-fluids courses and applied engineering related to building science, HVAC in particular. My undergraduate research ambition was to quantify the human-emitted volatile organic compounds from an indoor air quality perspective, and to understand how the linear combinations of the chemicals define a person's aromatic identity. Based on this research, I was awarded the *Best Thesis Award (2014)* in Tsinghua University. I was also involved with many thermal comfort, indoor air quality, ventilation modeling and HVAC research projects during my undergraduate. Since coming to MIT, I have had the opportunity to delve into many fundamental thermo-fluids studies and work with Prof. Leon Glicksman in Building Technology Lab on the applications of natural ventilation with a focus on bi-directional natural ventilation through CFD modelling. My other research participation includes understanding how radiative heat transfer affect the thermal stratifications in buildings, designing thermally automotive houses for highly constrained environments (India), as well as natural convection induced low-cost fish pool design. I also had the opportunities for being a teaching assistant for both undergraduate and graduate levels of classes at MIT.

Please send questions or comments to the author at:

qinzhang@mit.edu or qinzhang@alum.mit.edu

Contents

LIST OF TABLES AND FIGURES

Chapter 1

Chapter 3

Chapter 4

Chapter 5

Chapter 6

1. INTRODUCTION

1.1 Why natural ventilation?

More than 40% of energy consumption in the U.S [1] is due to buildings, as is shown in Figure 1-1. As an important component of building energy usage, heating, ventilating and air-conditioning (HVAC) comprises more than 1/3 of total energy consumption in buildings in the U.S and Europe [2], shown in Figure 1-2 and Figure 1-3. Such heavy energy consumption is undesirable due to the dwindling fossil fuel supply as well as the environmental impact, in terms of pollution and climate change, of burning fossil fuels. These concerns have promoted serious consideration of clean and high efficiency strategies in buildings.

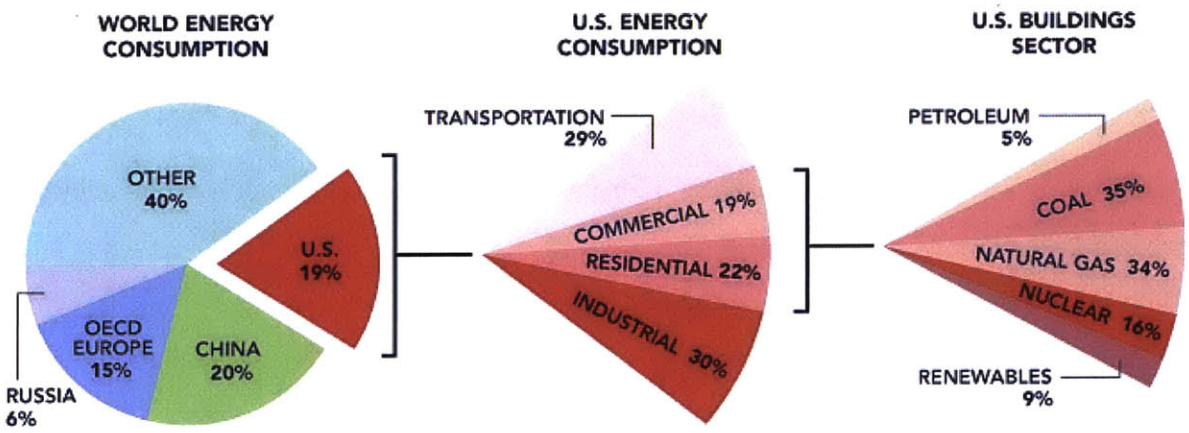

Figure 1-1. US building energy consumption composition

Besides economic and environmental considerations, the predominance of HVAC systems in modern buildings has resulted in serious health issues. Studies have shown that the use of HVAC systems does not necessarily create a healthy and comfortable environment: Stuart and Harriet reviewed literature on HVAC systems as contaminant emission source that affect indoor air quality and concluded that moisture can introduce bio-aerosol and VOC (volatile organic compounds) [3]; at the same time, the lack of fresh outdoor air leads to questionable air quality [4]. Hence, the

trend of 21st century building technology is to adapt and utilize the outdoor environment to create a healthy, productive, and thermally comfortable indoor environment.

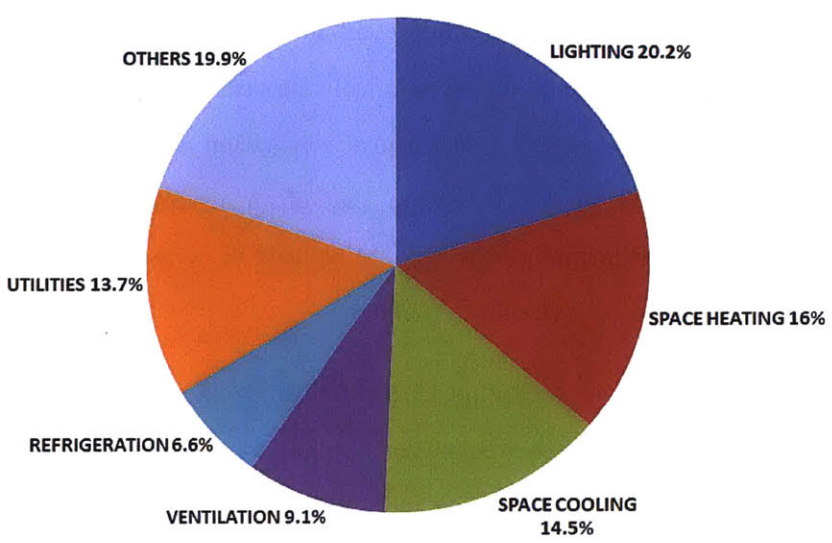

Figure 1-2. 2010 Commercial energy end-use splits (Primary energy).

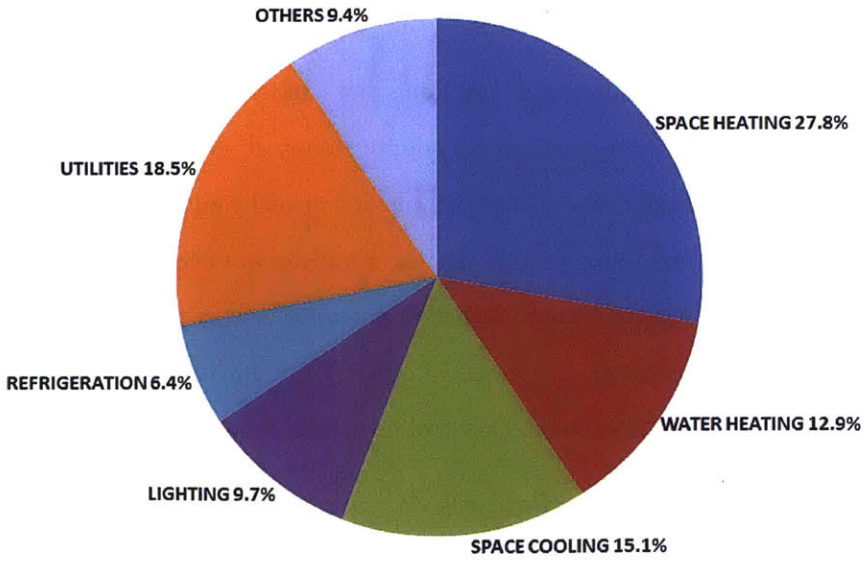

Figure 1-3. 2010 Residential energy end-use splits (Primary energy).

One of the most promising sustainable technologies for buildings is natural ventilation. It is not a novel technology since almost all historic building were ventilated naturally when there were no mechanical systems. Studies have shown that natural ventilated buildings have the great potential to be used reliably in most climates when combined with a mechanical system using the hybrid (mixed-mode) ventilation principle [5], even in cold climate such as Russia [6]. In favorable climates and building types, it is reported that natural ventilation can completely eliminate the air-conditioning plants, saving up to 40% less than that of an air conditioned building [7]. An additional benefit of natural ventilation is that it could be used to access higher levels of daylight since it encourages the buildings to have more openings.

Moreover, natural ventilation is highly praised because it is environmental friendly and economicly beneficial because it utilizes free natural forces for cooling and ventilating. Using natural ventilation also contributes to improving indoor air quality by introducing more fresh air into the buildings, if the outdoor environment is clean enough. It's reported by studies that natural ventilated buildings have higher rates of indoor air quality [8], thermal comfort [9] and thus working productivity [10]. Therefore, natural ventilation is becoming a more and more popular sustainable building technology thanks to its non-trivial energy-saving, environmental-friendly and productivity-increasing potentials.

The potential barriers, challenges and problems for understanding natural ventilation is fundamentally different from mechanical ventilating systems. It is rather difficult to design or control natural ventilated buildings due to the complexity of real buildings, lack of reference data and because natural ventilation relies largely on the ambient environment which is constantly changing. To predict and control natural ventilation accurately, it is essential to understand the fundamentals of the physical process. Emphasis should be put on understanding, the physics of natural ventilation for better utilization and control of natural ventilation.

1.2 Why bi-directional natural ventilation?

Bi-directional natural ventilation is one of the most common but not well understood phenomenon because the ventilation is strongly related with thermodynamic conditions and

geometric factors. The variation in thermal conditions results in the ventilation forming a density stratified pattern such that buoyancy forces drive the flow to exchange in a bi-directional form at the same opening. The fact that the opening is both the inlet and outlet of ventilation simultaneously makes it rather difficult to characterize and understand the heat and mass transfer process.

Understanding and predicting the bi-directional natural ventilation is challenging due to the complex and time-dependent airflow pattern as well as the strong coupling effect between ventilation and temperature. For cross ventilation, theories for calculating ventilation performance have been well developed and validated by experiments [11]. Nevertheless, for bi-directional ventilation, a few investigations have been successfully launched, yet sufficient understanding is still lacking due to the multi-factor dependent nature of the process.

The simplest and most common scenario of bi-directional airflow is single-sided buoyancy-driven natural ventilation. It happens at a single opening where there is variation of thermal condition in each side of the opening. A non-dimensional discharge coefficient is a crucial parameter for estimating the ideal mass flowrates. Conventionally, the coefficient is assumed to be a constant of 0.62 [4], which has been proved to be problematic. Simulations and experiments have shown that the coefficient is largely dependent of zonal temperature difference [12,13] and geometrical factors [14]. However, consensus and knowledge are still lacking about the discharge coefficient.

The ventilation mode becomes more complicated in the presence of multi-zone and combined wind and buoyancy forces. The air flow pattern can change from bi-directional ventilation to unidirectional ventilation depending on the dynamics of wind and buoyancy forces, and the interaction of zonal pressure difference and thermal conditions.

The ventilation process might become even more complicated where heat sources exist. The thermal stratifications in buildings is largely affected by the type and number of heat sources. Paul Linden [15] pointed out that the transient effect is especially notable when the heat sources are not constant, which is often related with occupant behaviors. The typical time need for simple

room set-ups, such as an empty rectangular space, to reach a steady state is a few minutes, but the amount of time increases sharply when we consider complex interior geometry and thermal mass. Linden [16] also suggested from the calculations for a theatre of 500 people that the establishment for a complex real building environment can be an hour or so.

In conclusion, bi-directional ventilation is an essential natural ventilation mode for cases involving large buoyancy forces. It is critical to clarify and understand the ventilation behaviors of bi-directional airflow from global and transient points of view in order to accurately predict the natural ventilation performance to satisfy the air quality and thermal comfort requirements.

1.3 State of Art: single-sided buoyancy-driven ventilation

Single-sided buoyancy-driven natural ventilation is an important scenario in bi-directional natural ventilation where two spaces with different thermal conditions are connected through a single opening. The buoyancy forces drive the hot air to flow through the opening at the top half of the opening and the cold air to flow through the bottom half. Another example for single-sided buoyancy ventilation can be the air exchange through an interior opening that bridges a space and the ambient at different thermal conditions. This is often considered as the worst scenario in buildings where there is no wind in the environment and the openings are all at one side.

Theories and models have been established for single-sided buoyancy-driven ventilation. Emswiler [17] first applied Bernoulli's equation to obtain the heat and mass transfer through multiple openings in a wall. Brown and Solvason [14] then developed Emswiler's method to two-way flow through a single opening and established the analytical "natural convection" model (Equation 1-1) basing on the assumptions such that the flow is steady, non-viscous, fully developed, and that the neutral plane is located in the middle of the opening.

Equation 1-1: $$Q = \rho C_d \frac{W}{3}\sqrt{g\frac{\Delta\rho}{\rho}H^3} \text{ or } Nu_H = \frac{C_d}{3}Gr^{0.5}\,\mathrm{Pr}$$

In the equation, Q is the mass flow rate of the upper/bottom half of the opening, kg/s; W is the opening width and H is the height of the opening, m; ρ is the density of the air, and $\Delta\rho$ is the density difference of the two zones; g is the gravitational acceleration, m/s^2; C_d, is the discharge coefficient, defined in this model as the ratio of actual mass flowrate and ideal mass flowrate obtained from Bernoulli's theory; and Gr is the Grashof number, defined as a dimensionless number in fluid dynamics and heat transfer which approximates the ratio of the buoyancy to viscous force acting on a fluid; Pr is the Prandtl number, a dimensionless number defined as the ratio of momentum diffusivity to thermal diffusivity..

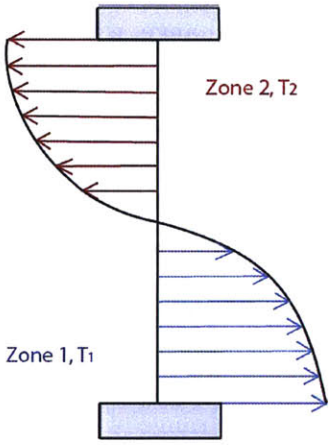

Figure 1-4. Schematics of bi-directional airflow through a single opening, T2>T1.

The original geometry they considered is shown in Figure 1-4, where two sealed spaces of different temperatures, T1 and T2, are separated by a single rectangular opening. Thus using ideal gas law, Equation 1-1 can be written using the temperatures of each zone as Equation 1-2,

Equation 1-2: $$Q = \frac{1}{3} C_d \cdot \rho \cdot A_{eff} \sqrt{2g \frac{|T_1 - T_2|}{T_1 + T_2} H}$$

The natural convection model is considered to be the most classical analytical model for single-sided buoyancy-driven ventilation given that it characterizes how buoyant forces affects

ventilation performance. Brown and Solvason [14] then conducted a series of experiments where two chambers containing air of constant but different temperatures were connected by a single rectangular opening whose height ranged from 3 to 12 inches. The discharge coefficient for difference cases were found to range from 0.6 to 1.0. The test results also suggested that the exponent on the Grashof number in Equation 1-1 was slightly greater than 0.5, which was attributed to the heat transfer mechanism by the authors. In their continuing work [18], they provided more specific correlations for different ranges of Grashof number.

Later in 1970th, more attention was paid to contaminant exchange and control. Shaw [19,20] conducted experiments in a hospital and measured air exchange between an isolation room and a vestibule to measure the density-driven air exchange, which in part reflected the spread of gaseous contaminants. The rooms were ventilated by a central system with air supply and extraction openings in each room with balanced air supply and extract volumes. Shaw found that the discharge coefficient was a function of the temperature difference, and it had a value of 0.66 when temperature difference ranged from 4K to 10K. In 1987, Barakat [21] wrote a comprehensive review on natural convection through a single opening regarding models obtained from different experiments. The recommended model was exactly the same form Equation 1-1 with a minor modification of the discharge coefficient to the range of 0.66 to 1.0. He also indicated that opening width had little effect on the discharge coefficient.

S. B. Riffat [22] examined the situation where ventilation was driven by temperature difference between the lower and upper floors in a residential house via an interior doorway. It was found by him that the discharge coefficient has a negative correlation with the temperature difference. In a later research followed by Wilson and Kiel [23], the heat and mass transfer between the ambient and a test house were measured on the exterior doorway for a very big range of temperature difference (0.5K – 45K). However, a positive correlation was observed in this experiment, which is contradictory to Riffat's findings.

In the recent 20 years, CFD simulation has been adopted to analyzing single-sided natural ventilation. Yi Jiang and Qingyan Chen [24] used two different turbulent models (RANS and LES) to simulate the buoyancy-driven single-sided natural ventilation between a test chamber and

laboratory environment. He validated the simulation with experimental measurements and found that LES model is more accurate than RANS model. However, in terms of understanding the discharge coefficient physically, this work is not that useful. In 2005, Favarolo and Manz [13] used CFD simulation to analyze the impact of geometrical configurations (dimensions and positions) and temperature difference on the air flow rate of single-sided ventilation between a room and the ambient. Six aspects were investigated, they are: temperature difference, distance from wall, opening width and aspect ratio, wall thickness, vertical position of the opening, and room depth and width. They also addressed the necessity and importance of extending available studies for rectangular opening to more complex commercial windows.

On the other hand, attentions were also paid to the single-sided buoyancy-driven natural ventilation through commercial window openings with complex geometries rather than plain rectangular openings. For openings with more practical relevance, the stratification is also affected by window characteristics. Jörn von Grabe [25] measured and compared the ventilation performance of almost 6 commercial types of windows (double vertical slide window, turn window, tilt window, awning window, and horizontal and vertical pivot windows) under pure buoyancy ventilation in a test chamber in controlled laboratory environments to control boundary conditions and eliminate wind impact. It was found that the horizontal pivot window had the best performance with the same initial set-up and opening area. He also proposed a method in a later paper [26] for estimating the ventilation performances for complex geometry windows. But the method seems to be problematic and difficult to implement in real engineering calculations and predictions.

To conclude, the major problems about single-sided buoyancy-driven natural ventilation lies in the value of the discharge coefficient, as well as how to apply the "natural convection model" to more complex but more practical commercial window geometries.

1.4 State of Art: combined wind and buoyancy ventilation

Mathematically, it was proved that the governing equations for the natural ventilation process sometimes contains two or more stable solutions [27-29] assuming unidirectional airflow pattern. Helselberg et al. [30] presented both experimental and computational evidence of the existence of multiple solutions in simple buildings. It was also found that initial conditions might play an important role in determining the steady state solution [31] for multi-zone building configurations.

However, these findings were challenged because they neglected the existence of bi-directional flow pattern. Shuangping Duan and Yuguo Li [32] used computational methods that took bi-directional airflow pattern into account and observed that the assumption of unidirectional airflow was in fact invalid and led to the existence of multi stable solutions.

An easy-to-understand example is a heated room with two opposite openings, one connecting with a cold chimney and one facing a cold ambient at the same temperature with the chimney. Initially, there is single-sided buoyancy ventilation with bi-directional flow due to the temperature difference between the room and the other two zones. As the chimney gradually heats up, there establishes a pressure difference between the ambient and the chimney is established such that it overwhelms the local buoyancy forces and drives the air to flow in a unidirectional pattern. However, if we neglect the initial bi-directional ventilation, the ventilation will not happen in theory since there is essentially no pressure difference between the ambient and the chimney.

Therefore, one of the most challenging unsolved problems is to understand the dynamics of bi-directional airflow and allow bi-directional patterns in natural ventilation estimation so as to derive at accurate solutions. On the other hand, in Shuangping Duan and Yuguo Li's work [32], they validated that initial conditions would largely impact the final steady state solution. However, they did not consider cases with unsteady heat sources. It is reasonable to assume that a change in the boundary condition or heat source might also contribute to the steady state solutions since buildings are dynamic and interactive environments, especially for multi zone buildings.

1.5 Thesis objectives

The aim of this work is to simulate the bi-directional flow pattern under pure buoyancy force or combined wind and buoyancy forces through computational fluid dynamics simulation, and to grasp some physical insight of the process while taking all the influencing factors into consideration, especially discharge coefficient as well as the dynamics of the bi-directional natural ventilation. To elaborate, this work aims to:

- To use computational fluid dynamics (CFD) simulation to visualize and understand how bi-directional airflow establishes and develops under two important scenarios:
    - Single-sided ventilation for two zones connected with a single rectangular opening.
    - Bi-directional flow through multi-zonal ventilation under combined buoyancy and wind forces for a heated room connecting with an atrium.
- To understand and explain the contradictory conclusion in the available literature on the discharge coefficient for single-sided natural ventilation, and to generate useful knowledge about the discharge coefficient regardless of its multi-factor dependent nature.
- To characterize the features of bi-directional natural ventilation for both multi-zone and two-zone model under different driving forces.
- To build a simplified model with acceptable accuracy for predicting the bi-directional flow, and to integrate the results into the fast natural ventilation design tool "CoolVent".

1.6 Structure of thesis

The current chapter (Chapter 1) is the introduction about the state of art for bi-directional natural ventilation with a highlight on single-sided buoyancy-driven natural ventilation. It covers

the existing methodologies, analytical models and experimental results for natural ventilation, bi-directional airflow in particular. It also discusses the unsolved problems in previous literatures.

Chapter 2 explains the fundamentals of bi-directional natural ventilation including driving forces, mechanisms for single-sided buoyancy-driven natural ventilation, combined wind and buoyancy ventilation, as well as unsolved problems of multi-zonal natural ventilation. Chapter 3 presents the methodology and simulation results for single-sided buoyancy-driven natural ventilation. The discharge coefficient (Cd) is studied intensively under various boundary conditions. A new concept called "local discharge coefficient" is proposed and compared with the traditional discharge coefficient. As an extension of Chapter 3, Chapter 4 explores the effect of radiation on the ventilation performance and thermal stratifications of single-sided buoyancy-driven natural ventilation. Thus, ignoring the effect of radiation was found to be associated with inaccurate thermal stratification profiles, air mass flowrates and surface temperatures in the room.

Chapter 5 gives the simulation results of a heated room connected with the ambient and a cold atrium. There are two opposite openings, one is connected with the ambient and another is connected with the atrium. Ambient wind can be applied such that there are combined wind and buoyancy forces. The transition from bi-directional airflow to one-directional airflow is observed and presented. The dynamics of thermal and wind pressure is investigated. Based on the simulation results, Chapter 6 proposed a simplified modelling framework that captures the features of both models to predict the transient thermal and ventilation behaviors of both models that is to be implemented to the natural ventilation tool "*CoolVent*". Assumptions (lumped approximation, discharge coefficient, etc.) are made so as to simplify and approximate this process.

Chapter 7 presents conclusions from the previous-mentioned work on bi-directional natural ventilation and addresses the limitations of this work. Further work needed is also identified in this chapter.

2. FUNDAMENTALS OF BI-DIRECTIONAL NATURAL VENTILATION

2.1 Driving Forces of Natural Ventilation

Natural ventilation is the process of utilizing natural forces to remove excess heat and gaseous pollutants from an indoor space without using mechanical ventilating systems. The natural forces give rise to the zonal pressure difference that causes air to exchange and ventilate.

Conventionally, there are two major driving forces for natural ventilation: wind forces and buoyancy forces. The wind forces induce a positive pressure on the windward face and negative pressure on the leeward face so that it drives air to flow through the windward openings into the buildings at a lower pressure. The buoyancy forces are generated from the thermal variations between one zone and another. The variation causes a different vertical pressure gradient that drives air to ventilate.

To accurately predict natural ventilation, these forces should be quantified through simple but well-defined equations. Heiselberg [1] gives a general equation for wind pressure that takes wind velocity, wind direction and incidence angle into consideration.

$$\text{Equation 2-1: } \Delta P_{wind} = \frac{\rho}{2} \cdot f(\beta)^2 \cdot |C_p| \cdot U_R^2$$

where $f(\beta)$ is a function depending on the incidence angle, C_p is the pressure coefficient and U_R is the wind velocity (m/s).

To be noted, the above equation is hard to use for cases where the directional of wind is not orthogonal to the opening. The angles between the wind direction and the opening will influence the wind pressure coefficient. Since this work is mainly focused on not the driving forces but the bi-directional airflow, we only considered scenarios where the wind direction is orthogonal to the opening thus the wind pressure is simply a function of velocity and air density,

Equation 2-2: $\Delta P_{wind} = \frac{\rho_{ambient}}{2} u^2$

On the other hand, Warren and Parkins [2] gives an expression for buoyancy-driven pressure based on the Bernoulli equation,

Equation 2-3: $\Delta P_{thermal} = 2 \cdot \frac{T_{zone1} - T_{zone2}}{T_{zone1} + T_{zone2}} \cdot \rho g \cdot \Delta H$

where T_{zone1} and T_{zone2} are the reference temperatures of two spaces, and ΔH is the vertical difference of the centerline height of the spaces.

In the presence of combined wind and buoyancy forces, the contribution of both wind and thermal buoyancy should be taken into consideration. Thus, the total mass flowrate (one-directional only) can be calculated from the orifice equation,

Equation 2-4: $m = \rho C_d \cdot A_{eff} \cdot \sqrt{2\rho \cdot (\Delta P_{wind} + \Delta P_{thermal})}$

In the above equation, A_{eff} is the effective opening area, the rest of the parameters have been explained previously. Similar equations can be derived for cases involving only wind or thermal pressure. However, this equation (Equation 2-4) uses the averaged pressure difference rather than integrating the pressure difference across the height between the inlet and outlet to calculate the mass flow rate. It neglects the fact that the profiles of wind pressure and stack pressure are different: the wind pressure generally results in a constant pressure difference across the opening while the stack pressure results in a linear pressure difference. This is most obvious in single-sided buoyancy-driven natural ventilation where the integration of the stack pressure across half of the opening height results in a 1/3 coefficient. That is to say, the definition of discharge coefficient for single-sided buoyancy ventilation and combined wind and buoyancy ventilation is different.

2.2 Mechanisms of Single-sided Buoyancy-driven Ventilation

As previously mentioned, the most classic model for single-sided buoyancy-driven ventilation is the "natural convection model". The driving force of single-sided buoyancy-driven ventilation is the buoyancy forces induced by the temperature differences between zones at a different temperature.

The "natural convection model" is based on the assumption that the ventilation is fully turbulent. However, in favorable climate or ventilation inside buildings, the temperature difference between zones is usually less than 10 K. The momentum of air generated by the buoyant plume is quite small compared to the buoyancy forces, yielding a mild and slow ventilation process compared to mechanical ventilating or wind-driven natural ventilation. In that case, the mass flow rate is correlated with the pressure difference with an exponent in between 0.5 to 1.0, 0.5 being fully turbulent and 1.0 being laminar. This results in the discharge coefficient to be dependent on pressure difference rather than being a constant.

On the other hand, from the perspective of fluid morphology, two most important features of single-sided buoyancy-driven natural ventilation are that the flow pattern is bi-directional and that the mass flowrate at each direction should be equal due to mass conservation. The simplest case is the ventilation through a plain rectangular opening. However, for commercial window openings with complex geometries, using plain rectangular opening is not an ideal approximation because the flow pattern becomes highly 3-dimensional and the flow resistance is a function dependent on opening geometries and angles rather than merely a constant.

Mathematically, nondimensionalization can be applied to characterize the relationships between the buoyancy forces, inertia and viscous forces. Two non-dimensional groups are commonly used for single-sided buoyancy ventilation: Grashof number (Gr) and Archimedes number (Ar). Their definitions are as follows:

$$\text{Equation 2-5: } Gr = \frac{g\beta(T_{zone1} - T_{zone2})D^3}{v^2} = \frac{Buoyancy}{Viscous}$$

Equation 2-6: $$Ar = \frac{g\beta(T_{zone1} - T_{zone2})D}{V^2} = \frac{Gr}{\mathrm{Re}^2} = \frac{Buoyancy}{Inertia}$$

where β is the coefficient of thermal expansion (equal to approximately 1/T, for indoor air), 1/K; D is the hydraulic diameter of the opening; V is the external flow velocity, m/s^2; ν is the kinematic viscosity, m^2/s. For single-sided buoyancy-driven ventilation, we expect the Grahof number to be large and the Archimedes number to be a small value.

2.3 Mechanisms of Bi-directional Airflow for Multi-zonal Ventilation

Predicting natural ventilation for a multi-zone system has always been challenging due to the complexity of multiple driving forces, building geometries, and inter-zonal interactions. The most important criteria of bi-directional multi-zonal ventilation are mass and energy conservations. For multi-zone natural ventilation, unidirectional flow assumption is usually made for simplicity for conventional flow network model. This is based on considerations that bi-directional flows only happens in limited cases such as single-sided ventilation and around the neutral plane of a building.

However, Nitta [3] modified the numerical network model of bi-directional flows in a building by assuming the neutral plane height is located near the middle height of the building. This model successfully characterized the bi-directional flow of a building at the steady state. However, this model is only focused on steady state solutions and fails to model the transient flow behaviors of bi-directional flows.

3. LOCAL DISCHARGE COEFFCIENT: A NEW CONCEPT FOR SINGLE-SIDED BI-DIRECTIONAL NATURAL VENTILATION

Abstract: The discharge coefficient for the bi-directional single-sided buoyancy-driven natural ventilation is a critical but not-well-understood number due to its widely varying nature under different conditions. To understand the discharge coefficient, we use computational fluid dynamics to simulate two typical scenarios (room-room/room-ambient) under different boundary conditions (heated wall/heater). We find that thermal stratification causes zonal thermal conditions to deviate from local thermal conditions at the opening, whereas the discharge coefficient is traditionally defined by zonal temperature difference. A new concept—the *local discharge coefficient*—is put forward that shows better consistency under various boundary conditions than the traditional discharge coefficient.

3.1 Introduction

Natural ventilation is a promising sustainable design strategy thanks to its significant potential in saving energy [1], improving indoor air quality [2] and boosting working productivity [3]. Single-sided buoyancy-driven natural ventilation is an important scenario where two spaces with different thermal conditions are connected through a single opening [4-6]. Two important cases are: 1) air exchange between two indoor spaces; 2) air exchange between a windless environment and a room.

The natural convection model [7] is the most well established analytical model for the single-sided bi-directional buoyancy-driven natural ventilation. It is based on Bernoulli's principle by assuming that the flow is steady, non-viscous, fully developed, and that the neutral plane is located at the middle height of the opening. A critical number, the discharge coefficient, is introduced to characterize the ratio between the real and ideal mass flow rates:

Equation 3-1: $$Q = \rho C_d \frac{W}{3}\sqrt{g \cdot \frac{\Delta T}{\overline{T}} \cdot H^3}\ ,$$

where Q is the mass flow rate, kg/s; C_d is the discharge coefficient; W is the width, m; ρ is the density of air, kg/m^3; ΔT is temperature difference between the two zones, K; $\overline{T}$ is the average temperature of the two zones, K; H is the height, m; g is the gravitational acceleration, m/s^2.

Brown and Solvason [8] conducted a series of experiments where two chambers containing air of constant but different temperatures were connected by a rectangular opening with a height ranging from 3 to 12 inches. The discharge coefficient for different cases was found to vary from 0.60 to 1.00. Field measurements also suggested that the discharge coefficient is very case-dependent: Shaw [9] measured the buoyancy-driven air exchange between an isolation room and a vestibule in a hospital to study the spread of gaseous contaminants. He found that the discharge coefficient was dependent on the temperature difference. Later in 1987, Barakat [10] suggested a range of discharge coefficients of 0.66 to 1.00 in his comprehensive review on the natural convection through a single opening.

It is also unclear how temperature difference affects the discharge coefficient within the same configuration. S. B. Riffat [11] examined the ventilation between the lower and upper floors in a residential house via an interior doorway and found that the discharge coefficient was inversely correlated to temperature difference. However, Wilson and Kiel [12] measured the air exchange between the ambient and a test house through an exterior doorway and observed a positive correlation.

Therefore, this chapter is designed to develop an understanding of how the discharge coefficient of single-sided buoyancy-driven natural ventilation reacts to various factors such as temperature difference, boundary conditions and geometric factors so as to derive at an understanding for the above-mentioned confusion and contradictions. We suggest an explanation for the widely varying nature of the discharge coefficient from CFD results, and propose a new concept of the local discharge coefficient that has better consistency under different boundary conditions than the traditional discharge coefficient.

3.2 Methodology

3.2.1 Room-room model

A room-room computational model is built by connecting two spaces of the same size with a rectangular opening, shown in Figure 3-1a.

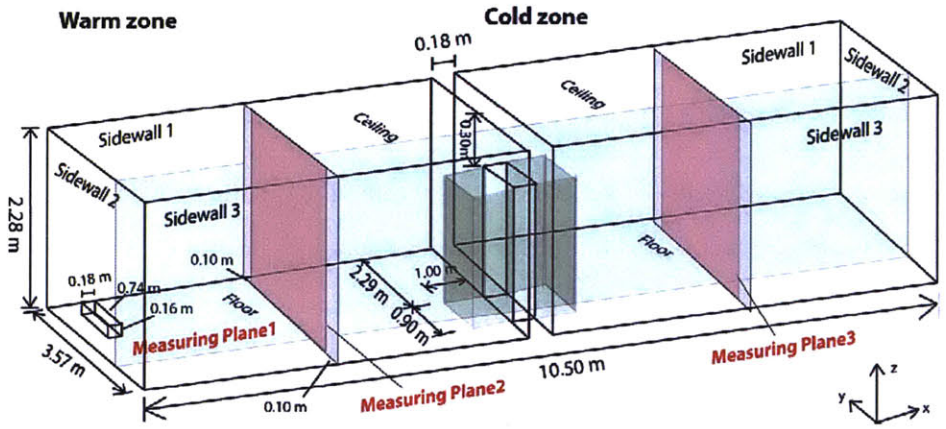

(a)

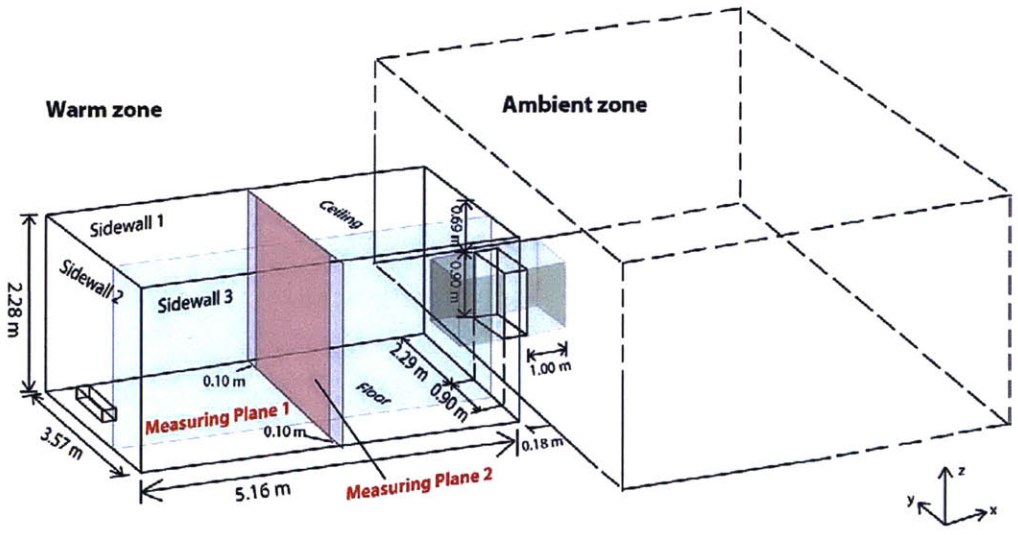

(b)

Figure 3-1. Domains of the room-room model with a door opening (a) and the room-ambient model with a window opening (b). The measuring planes are indicated in the figures.

Each room is 3.57 m deep, 5.16 m long and 2.28 m high. A surface heater is implemented as a cuboid (0.16 m high, 0.74 m wide and 0.18 m high) near the corner in the warm zone. A single

plain rectangular opening is created in the wall that connects the warm and cold zones. Two types of openings are modeled: a door (1.98 m high, 0.90 m wide and 0.18 m thick) and a window (0.90 m high and 0.90 m wide). Three vertical measuring planes are created to measure the thermal stratification patterns at different spatial locations. Two of the measuring planes (plane 2 and plane 3) are located in the middle of each zone, parallel to the opening and 10 cm from the sidewalls on each side to avoid the inference of the side walls. The other plane (plane 1) is orthogonal to the opening across the entire domain, as is shown in the figure. The geometry of each room is adapted from a previous experimental work by Yi Jiang and Qingyan Chen [13].

The influence of thermal factors is explored by controlling the boundary conditions of all the simulated cases. Two sets of boundary conditions are considered: 1) heated sidewalls with constant temperatures, and 2) a heater with constant heat flux. For the first set of boundary conditions, the sidewall temperature of the cold zone is set at a reference temperature (T_{ref}) of 20.0 °C, and that of the warm zone is set at a higher temperature ranging from 21.0 °C to 30.0 °C. The ceiling and floor in each zone are modeled as adiabatic. For the second set of boundary conditions, the heater is turned on with a constant power ranging from 100 W to 500 W. The steady state heat fluxes from the sidewalls in each zone with fixed wall temperatures of 30.0 °C for the warm zone and 20.0 °C for the cold zone are approximately 500 W so that the ranges of heat intensity for the two sets of boundary conditions are comparable. The cold zone sidewalls are set at 20.00 °C. The other surfaces are modeled as adiabatic. By applying proper surface temperatures/heater powers, a small zonal temperature difference of less than 7.0 °C between the warm and cold zone is created.

Each case is simulated using FLUENT (part of ANSYS 14.5) in steady-state mode until the ventilation rate and thermal stratification stabilize. The turbulence model used is RNG k–ϵ. This turbulence model has been shown to accurately simulate room airflow dynamics [14]. The radiation model is the S2S model. All surfaces are modeled with an emissivity of 1.0. This simplification is justified given that typical materials in a room, excluding polished metals, have emissivity above 0.9 [15]. The ideal model was used for air. The closest node to all surfaces is at distance of 2 cm, with $y^+ \lesssim 5$ in accordance with the enhanced wall function. The above-mentioned numerical

method is validated through reproducing the experimental results obtained by Yi Jiang and Qingyan Chen [13]. Thermal stratification patterns are shown as contour plots of excess temperature relative to the reference temperature (T_{ref}) of the side walls in the cold zone, which is 20.0 °C. The temperature contours are plotted for each of the three measuring planes in each case. Bulk temperature is calculated as a volume averaged temperature of each zone and is used to define the discharge coefficient, as in Equation 3-1.

3.2.2 Room-ambient model

A room-ambient model to study the flow dynamics between the ambient and a heated room is built by enlarging the cold zone to a considerably larger size (10 m wide, 10 m long and 10 m high), and is shown in Figure 3-1b. The room geometry as well as the boundary conditions are maintained the same as in the room-room model. In the ambient zone, the three surrounding sidewalls are set as pressure inlets and the ceiling is set as a pressure outlet. All the mentioned surfaces in the ambient zone are set at 20.0 °C and the floor is modeled as an adiabatic no-slip boundary. The connection wall between the ambient and the room is modeled as adiabatic. The same window and door openings are modeled. The same meshing methods and radiation model as the room-room model are adopted for the simulation. Bousinesq approximation is used for the air. Two vertical measuring planes are inserted: plane 2 is located in the middle of the room in parallel to the opening with a 10 cm distance from the side walls on each side, and plane 1 is orthogonal to the opening, shown in Figure 3-1b.

Pressure interpolation is achieved using the "PRESTO!" (PREssure STaggering Option) scheme, while the velocity--pressure coupling is performed using the "SIMPLE" (Semi-Implicit Method for Pressure-Linked Equations) algorithm. Spatial discretization of the governing equations is achieved using a second order upwind scheme; the steady state formulation used is first order implicit. Similarly, the numerical method is applied to reproduce the work mentioned before [13] and shows good agreement with the experiment.

3.3 Results

3.3.1 Room-room model

3.3.1.1 Thermal stratification

As previously mentioned, two boundary conditions are considered: fixed sidewall temperatures of both zones (fixed wall temperature, FWT), and a heater with constant powers in the warm zone (fixed heat flux, FHF). Figure 3-2 shows contour plots of the excess temperatures for both boundary conditions from the middle measuring plane (plane 1) for the room-room scenario. The zonal temperature differences are similar between the different heat sources (door: $dT_{FWT} = 3.0$ K, $dT_{FHF} = 2.5$ K; window: $dT_{FWT} = 5.0$ K, $dT_{FHF} = 5.3$ K) and thus we can neglect the influence from temperature difference and the type of heat source is the main factor influencing the ventilation performance.

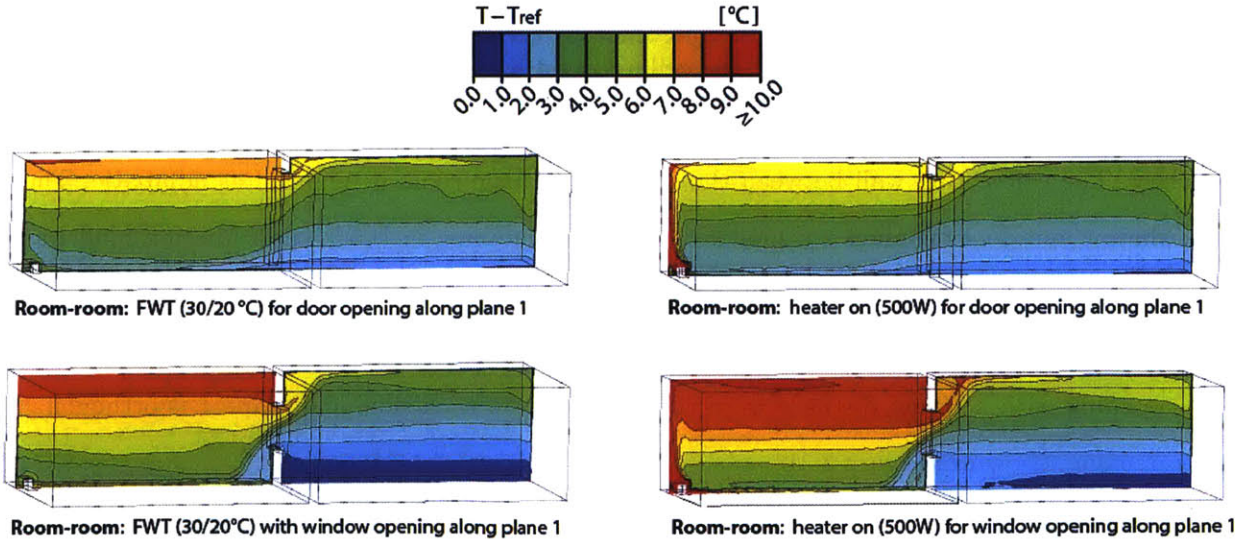

Figure 3-2. Contour plots of excess temperature for door (top) and window openings (bottom) in the room-room model, when the sidewalls are fixed at 20. 0 °C/30. 0 °C (right), and when there is a heater (500 W) in the warm zone and the cold zone sidewall temperature is fixed at $T_{ref} = 20.$ 0 °C (right). Excess temperatures above 10.0 °C are shown in red.

As is shown in Figure 3-2, single-sided buoyancy-driven natural ventilation is established for both FWT and FHF cases, yet by different mechanisms: 1) for the FWT cases, thermal plumes

are generated due to the convective heat exchange with the sidewalls in the warm zone, whereas 2) for the FHF cases, the ventilation is dominated by a high-momentum high-temperature plume from the heater surfaces. Therefore, the buoyant plumes are uniformly generated by the heated walls in the FWT cases but concentrated from the heater region in the FHF cases. We thus name the two flow types "bulk flow" and "plume jet flow" for simplicity. It should also be noted that single-sided buoyancy-driven natural ventilation with a large opening is less influenced by the non-uniformity of the heat source than with a smaller opening, shown in the Figure 3-2. For the door opening, the thermal stratification patterns are essentially the same between FWT and FHF boundary conditions. However, for the window opening, the thermal stratifications exhibit different features under different types of heat sources: 1) a linear thermal stratification is still observed with the FWT boundary condition, however, 2) with the FHF boundary condition a considerably thick hot air layer starts to accumulate near the ceiling and there are skewed temperature contours.

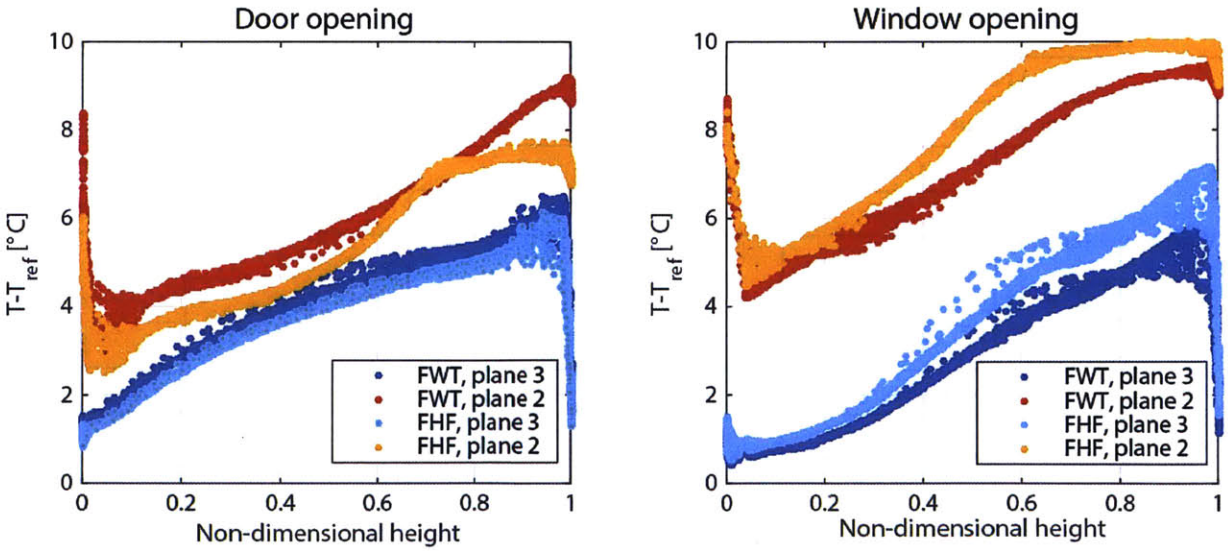

Figure 3-3. Vertical distribution of excess temperature above the reference temperature in the four cases in Figure 3-2, along two planes 2 and 3 in the room-room model, for the door opening (left) and window opening (right).

Figure 3-3 presents the vertical temperature distributions in measuring planes 2 and 3 in the room-room model for "bulk flow" and "plume jet flow" for both opening geometries (door/window). At each height, the temperature is plotted for all of the nodes in the CFD simulation across the

width of each room. The temperature distributions of the sampling nodes in each plane are located tightly in thin lines, indicating that there is little temperature variation along the y-axis within the same measuring plane. It is also observed that the window case presents a substantially larger temperature difference between the cold and warm zones than the door under the same boundary conditions. For the door opening, the larger mass flow rate causes more heat exchange between the two zones such that the zonal temperature difference is dampened.

It is also noted that the ceiling and floor temperatures of each zone approach each other because of the radiative heat transfer between surfaces, regardless of thermal stratification patterns. Therefore, the cold zone ceilings are of low temperatures and the warm zone floors are of high temperatures and there are temperature drops at these places. To illustrate this, Table 3-1 shows the area-averaged temperatures of the surfaces in each case.

Table 3-1. Surface temperatures of the floor, ceiling, connecting wall and sidewalls for the room-room cases in Figure 3-2.

Boundary conditions		**FWT**		**FHF**	
Opening types		Window	Door	Window	Door
Warm zone surface temperatures [°C]	Ceiling	29.1	28.9	29.4	27.1
	Floor	28.0	27.8	28.5	26.5
	Sidewall 1	30.0		28.3	25.8
	Sidewall 2			30.7	28.2
	Sidewall 3			28.8	26.4
	Connecting wall	28.3	28.2	28.2	26.1
Cold zone surface temperatures [°C]	Ceiling	22.1	22.6	22.8	22.1
	Floor	21.0	21.3	21.2	21.1
	Sidewalls	20.0			
	Connecting wall	21.8	22.3	22.3	21.9
Local temperature difference [°C]		4.5	2.4	4.8	1.9
Zonal temperature difference [°C]		5.0	3.0	5.3	2.5
Mass flowrate [kg/s]		0.067	0.124	0.070	0.116

The opening size seems to have a larger influence on surface temperatures for the FHF boundary conditions than the FWT boundary conditions: as we enlarge the size of the opening

from a window to a door, the temperature of each of the surfaces in the heated zone does not vary much (less than 0.5 °C) for the FWT cases, but changes substantially (more than 2.0 °C) for the FHF cases. Thermal non-uniformity is also observed in the three sidewalls in the FHF cases — sidewall 2 exhibits the highest temperature because it has a larger view factor to the heater than the other two sidewalls do and the thermal plumes rise along the sidewall 2. Meanwhile, the spatial distribution of heat source also largely affects the radiative heat transfer, surface temperatures and spatial temperature distributions. In the FWT cases, the large surface areas and view factors between surfaces contribute to more uniformly distributed surface temperatures, whereas in the FHF cases, the end wall in the warm zone has a larger view factor than the other surfaces in the heater cases, resulting in notable thermal non-uniformity along the x-axis in Figure 3-1.

3.3.1.2 Local temperature difference

The basic assumption for the *natural convection model* is that the temperature profile in each zone is uniform such that there is a constant temperature difference between the two zones. Conventionally, the discharge coefficient is defined by the zonal temperature difference. However, it is questionable whether the zonal temperature difference is appropriate to define the discharge coefficient due to the above-mentioned spatial thermal non-uniformity. Local thermal conditions near the opening might be more important. To investigate this, a local temperature difference is defined between the spatially averaged temperatures of the air in the cuboid regions within 1.0 m from the opening and across the entire opening height and width on either side of the opening, shown in Figure 3-1, to reflect the local thermal conditions. Figure 3-4 gives the zonal temperature difference and the local temperature difference in the room-room model.

The results suggest that the local temperature difference is generally smaller than the zonal temperature difference for all of the cases. This can be explained by the mixing of warm and cold air at the opening that homogenizes the temperature distribution across the opening region and results in a smaller local temperature difference than zonal temperature difference. Meanwhile,

the difference between the local and zonal temperature differences increase with the temperature difference for both door and window openings. Again, this is contributed to by the increased heat intensity which introduces thermal non-uniformity, i.e. when the heater power increases, the surface temperatures near the heater will be much higher than the rest of the surfaces, resulting in a larger deviation between the local and zonal temperature differences.

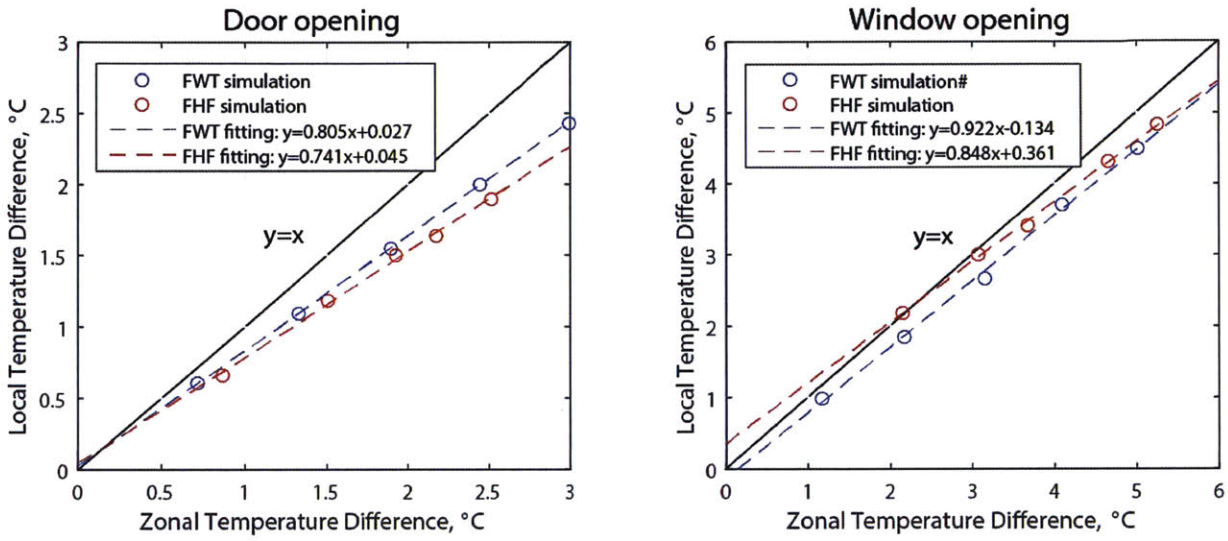

Figure 3-4. Zonal temperature difference and local temperature difference for room-room cases for door (left) and window (right) openings with FWT (blue) and FHF (red) boundary conditions. In the five different FWT cases, the warm zone sidewall temperatures are 22.0°C, 24.0°C, 26.0°C, 28.0°C, 30.0°C, and the cold zone sidewall temperature is 20.0°C. The heat fluxes for the five FHF cases are: 100 W, 200 W, 300 W, 400 W, and 500 W. The dashed lines are the fittings of the simulation results.

Another observation is that the deviation between zonal temperature difference and local temperature difference is larger for the door opening than for the window opening, suggesting that geometric factors can affect the correlation between the two temperature differences. One of the reasons for this observation is that increased opening area causes more mixing of cold and warm air at the opening, resulting in a larger difference between the local thermal conditions and the zonal averaged thermal conditions.

To conclude, the thermal stratification patterns are affected by the combination of heat source, heat intensity, opening sizes and other geometric factors, and the local thermal conditions is different from the zonal averaged temperature difference due to thermal non-uniformity.

3.3.2 Room-ambient model

3.3.2.1 Thermal stratification

Similar to the room-room model, the excess temperature contours of the FWT and FHF boundary conditions with both door and window openings are presented in Figure 3-5. The zonal temperature differences are also close for the same opening (door: $dT_{FWT} = 2.2$ K, $dT_{FHF} = 2.7$ K; window: $dT_{FWT} = 4.3$ K, $dT_{FHF} = 3.6$ K) so that the influence of temperature difference can be neglected.

Same ventilation mechanisms—"bulk flow" and "plume jet flow"—can be observed in the room-ambient case. Different from the room-room model, the thermal stratification in the room-ambient model is no longer horizontally layered but exhibits a wavy pattern. A bulk stream of ambient air penetrates deeply into the warm zone and is gradually heated up by the internal heat gains. As the opening size decreases from a door to a window, the bulk stream of cold air diminishes to a small stream. To understand how the thermal stratification in the room-ambient model is different from the room-room model, we plot the vertical temperature distributions in measuring plane 2 in Figure 3-6 for the four cases described in Figure 3-5. More horizontal thermal variations are observed than the room-room scenario and the temperatures of the sampling points are sparsely distributed in broader strands rather than thin lines, as is shown in Figure 3-6.

Similarly, a temperature drop near the floor in the room zone in each case is observed. Table 3-2 gives the area averaged surface temperatures in each of the four cases shown in Figure 3-5. Similar to the room-room model, the size of opening also has more influence on the surface temperatures for the FHF boundary condition than for the FWT boundary condition, and sidewall

2 exhibits the highest temperature compared to the other two sidewalls because of a larger view factor to the heater as well as the thermal plumes from the heater that heat sidewall 2.

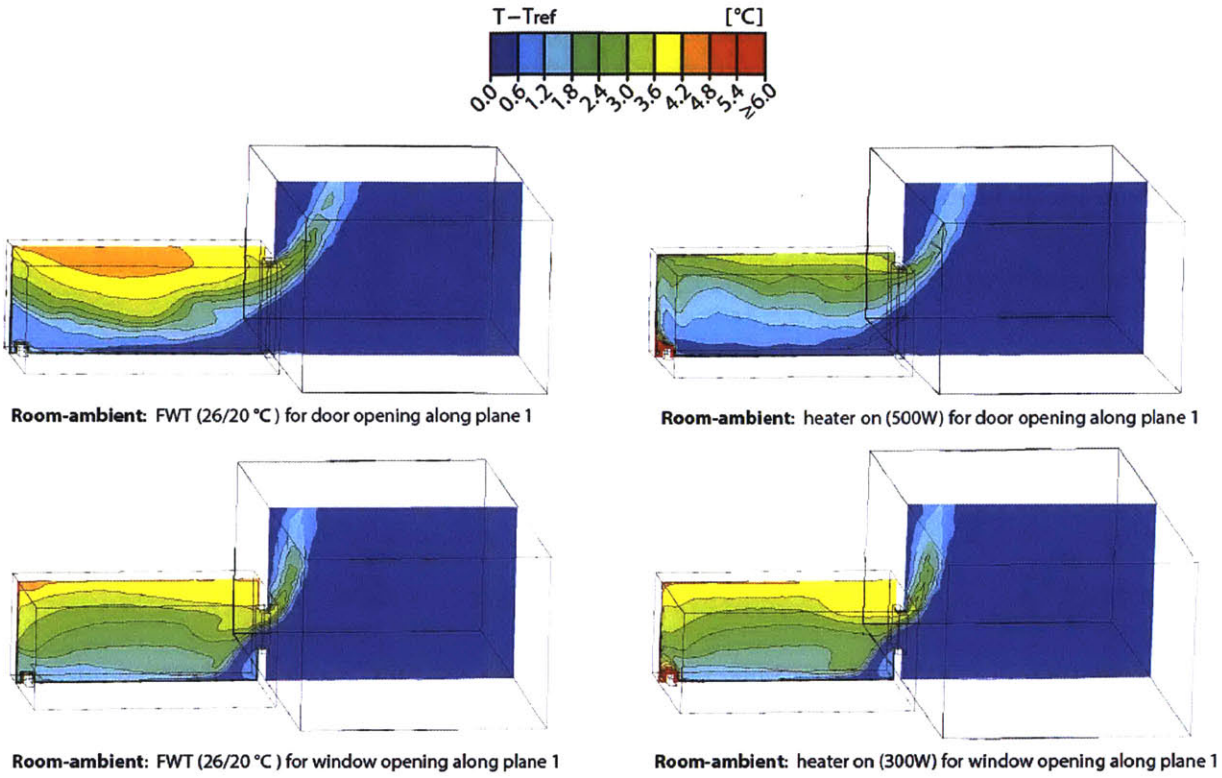

Figure 3-5. Contour plots of excess temperature for door (top) and window openings (bottom) in the room-ambient model along measuring plane 1, when the sidewalls are fixed at 20. 0 °C, 26.0 °C (left), and when there is a heater in the warm zone and the cold zone side wall temperature is fixed at T_{ref} = 20. 0 °C (right). Excess temperatures above 10.0 °C are shown in red. The size of the ambient zone is smaller than the real geometry for demonstration purposes.

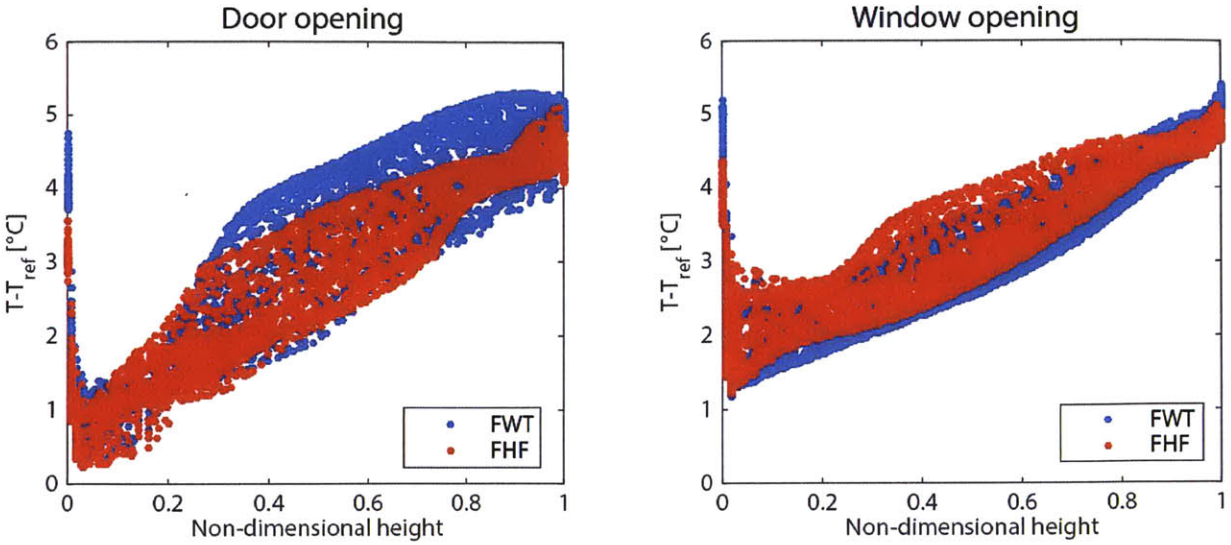

Figure 3-6. Vertical distribution of excess temperature along measuring plane 2 in the room-ambient models shown in Figure 3-5 (FWT (blue) and FHF (red) cases with door (left) and window (right) openings).

Table 3-2. Surface temperatures of the floor, ceiling, connecting wall and side walls for the room-ambient cases in Figure 3-5.

Boundary conditions		**FWT**		**FHF**	
Opening types		Window	Door	Window	Door
Warm zone surface temperatures [°C]	Ceiling	28.7	28.1	24.9	24.4
	Floor	27.2	26.3	24.5	24.0
	Sidewall 1	30.0		24.8	24.1
	Sidewall 2			26.1	26.0
	Sidewall 3			24.6	23.7
	Connecting wall	27.6	26.8	22.1	23.3
Ambient temperature [°C]		20.00			
Local temperature difference [°C]		3.7	1.9	3.7	1.9
Zonal temperature difference [°C]		4.3	2.2	3.6	2.7
Mass flowrate [kg/s]		0.092	0.202	0.073	0.162

3.3.2.2 Local temperature difference

Figure 3-7 gives the zonal temperature difference and the local temperature difference in the room-ambient model. Similar to what is observed in the room-room model in Figure 3-4, the larger opening (door opening) exhibits a larger deviation between the zonal and local temperature differences in the room-ambient model. For the door opening, the deviation increases as the temperature difference enlarges, whereas for the window opening the temperature difference has less impact on the deviation. In summary, the correlations between the two temperature differences are influenced by the types of heat source and size of the opening; the local temperature difference has more deviations from the zonal temperature difference for the large opening (door) than the small opening (window).

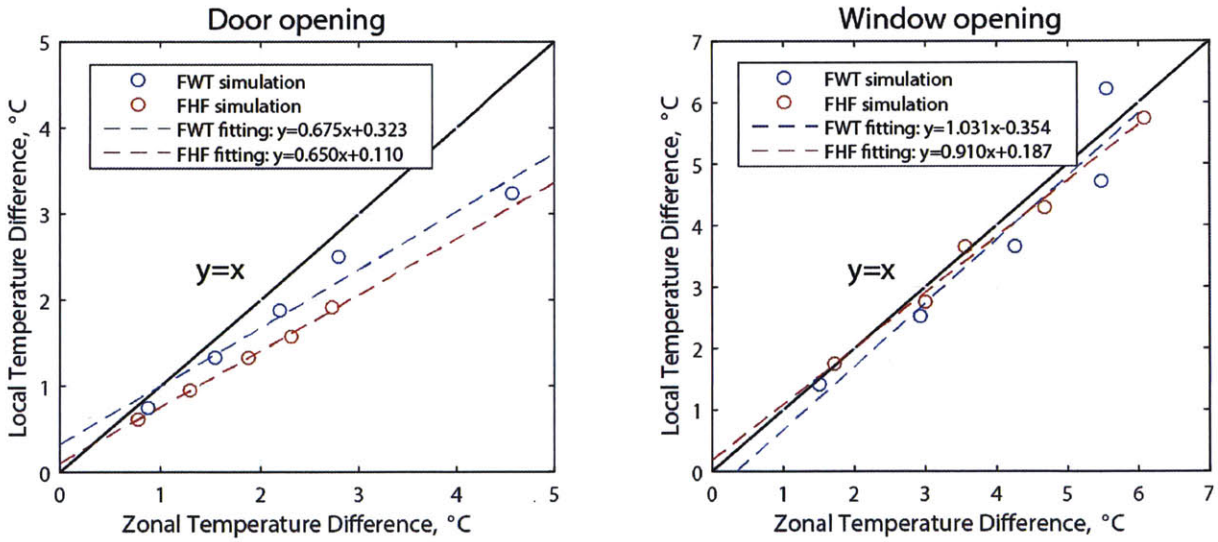

Figure 3-7. Zonal temperature difference and local temperature difference for room-ambient cases for door (left) and window (right) openings with FWT (blue) and FHF (red) boundary conditions. In the FWT cases, the warm zone sidewall temperatures are 22.0 °C, 24.0 °C, 26.0 °C, 28.0 °C, 30.0 °C, and the cold zone sidewall temperature is 20.0 °C. The heat fluxes for the FHF cases are 100, 200, 300, 400, 500W. The dashed lines fittings of the simulation results.

In general, it is safe to conclude that the zonal averaged thermal conditions are different from the local thermal conditions at the opening region for both the room-room model and the room-ambient model, especially under non-uniform heat source and large heat intensity.

3.4 Discussions

3.4.1 Local discharge coefficient

As previously mentioned, deviations between the zonal temperature difference and the local temperature difference arise due to different thermal stratification patterns. Hence, a possible explanation for the widely varying nature of the discharge coefficient in the previous work is that the traditional definition of the discharge coefficient neglects spatial thermal variations. For cases with non-uniform thermal conditions, the local temperature difference might be a better indicator of the buoyancy forces that drive the single-sided ventilation. To investigate this, we compared the local discharge coefficient, defined by the local temperature difference, and the traditional discharge coefficient for both openings under a small temperature difference (< 7.0 °C), as is presented in Figure 3-8.

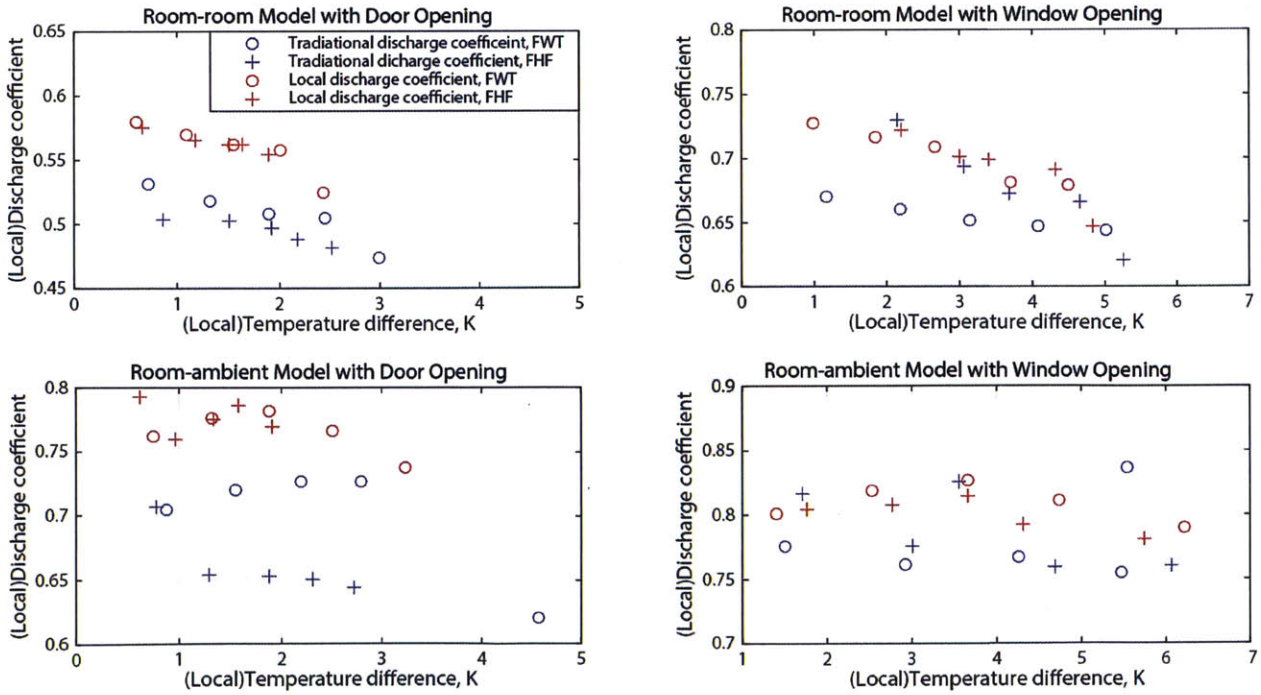

Figure 3-8. Comparison of the traditional discharge coefficient (blue) and the local discharge coefficients (red) for FWT cases (dot) and FHF cases (cross) for both room-room model (left) and room-ambient model (right).

The results suggest that the traditional discharge coefficient is dependent on both boundary conditions and temperature differences. This could be explained by the spatial thermal non-uniformity caused by different boundary conditions which gives rise to the difference between the local and zonal thermal conditions, as previously mentioned. However, the local discharge coefficient shows much better consistency than the traditional discharge coefficient under various thermal stratification patterns for both room-room and room-ambient scenarios. A direct implication is that the local temperature difference is less sensitive to the types of heat sources. Thus it is possible to eliminate the influence of thermal non-uniformity by using the local discharge coefficient. This is to say, for a given geometry, e.g. room-room with a window, the traditional discharge coefficient varies considerably (0.66 to 0.73) with the kind of heat source for the same temperature difference, whereas the local discharge coefficient eliminates most of this variation.

However, the local discharge coefficient still is a function of the geometry of the opening as well as the buildings. Under the same zonal/local temperature difference, the traditional/local discharge coefficient is of a higher value for the room-ambient scenario than the room-room scenario. Moreover, the local discharge coefficient in the room-ambient model seems to be more stable than the room-room scenario because the local discharge coefficient stays around the value of 0.80 under changing temperature differences as well as opening sizes (from door to window). This might result from the difference in the temperature distributions of the ambient zone in the room-ambient scenario and of the cold zones in the room-room scenario: the ambient zone is uniformly at 20.0 °C in the room-ambient scenario while there is thermal stratifications in the cold zone in the room-room scenario. In general, the local discharge coefficient is a function of thermal stratification patterns, opening geometries and temperature difference; the room-ambient scenario seems to have a more stable and lager local discharge coefficient than the room-room scenario.

3.4.2 Mass flow rate

Figure 3-9 shows the mass flow rate versus local temperature difference as well as their logarithmic values for the four sets of cases mentioned above. Linear correlations are observed between the logarithmic mass flow rates and logarithmic local temperature differences. It is noticed that the exponents in the correlations between the logarithmic mass flow rate and local temperature difference are between 0.435 and 0.480, while the natural convection model predicts the exponent to be 0.50. This could be explained by the fact that the local discharge coefficient is non-constant with different temperature difference and geometric factors.

It is noticed that the big opening (door) has substantially larger ventilation rates than the small opening (window) under the same local temperature difference. This is attributed to the fact that the increased opening area also reduces frictional loss, further improving the ventilation performance. It is also observed that the door case has a larger difference between the ventilation performances of the room-room and room-ambient scenarios than the window case has. Meanwhile, with the same opening, the room-ambient scenario exhibits a larger ventilation rate than the room-room model under same local temperature difference, which reflects the previous finding that the room-ambient cases have larger local discharge coefficients than the room-room cases under the same conditions. On the other hand, the correlation between the mass flow rate and the local temperature difference seems to be independent from the types of heat source because the cases with FWT and FHF boundary conditions are located in the same lines. This validates the point that local temperature difference is a better and more consistent indicator of buoyancy forces under different types of heat sources.

In conclusion, the mass flow rate is approximately square root of the local temperature difference regardless of the boundary conditions (FWT or FHF) since local temperature difference rules out the interference from boundary conditions. This relationship is essentially a reflection of the natural convection model which is stemmed from the Bernoulli's equation.

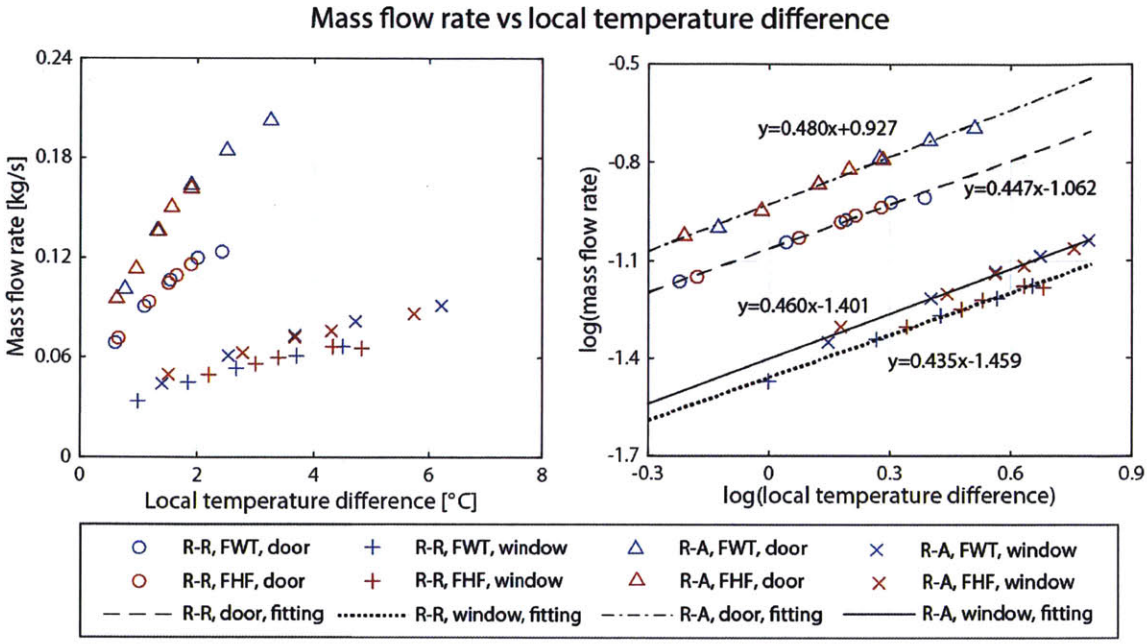

Figure 3-9. Comparison of the FWT (blue) and the FHF (red) for room-room (left) and room-ambient (right) models with door and window openings. R-A: room-ambient model; R-R: room-room model.

3.4 Conclusions

In general, this work investigated the role of thermal stratifications on the discharge coefficient and proposed a reasonable explanation for the controversy in the coefficient for single-sided buoyancy ventilation through extensive CFD simulations. We found that the single-sided buoyancy-driven ventilation is mainly dominated by local thermal and geometric conditions, and that different thermal stratification patterns will result in deviations between the local temperature difference and the zonal temperature difference. Therefore, the traditional discharge coefficient as defined by the zonal temperature difference is unable to accurately reflect the local thermal conditions, leading to its widely varying nature. Hence, we propose a new concept of the local discharge coefficient that is defined by the local temperature difference near the opening region. It is shown by CFD simulations that the local discharge coefficient shows better consistency

under various thermal stratification patterns for both room-room and room-ambient scenarios. It is considered to be a better gauge for estimating single-sided ventilation because it is able to rule out the influence of thermal stratifications, especially for buildings with localized heat sources.

However, the local discharge coefficient is still a function of temperature difference as well as geometric factors; more investigation is needed for thorough understanding. This suggests that using the typical value of 0.62 for the discharge coefficient might result in large errors in estimating the ventilation performance in single-sided ventilation. It is also observed that the discharge coefficients for FWT and FHF cases in the room-ambient model are relatively more stable than in the room-room scenario regardless of the change of opening geometry and temperature difference. This might be attributed to the fact that the ambient zone is at a uniform temperature, as well as the fact that there is less geometric restriction in the ambient zone.

4. EFFECT OF RADIATIVE HEAT TRANSFER ON SINGLE-SIDED BI-DIRECTIONAL NATURAL VENTILATION

Abstract: Scale models [1,2] and related theories [3,4] that ignore radiative heat transfer have been applied to studying airflow and thermal conditions in building. However, studies have shown that neglecting radiative heat transfer can lead to inaccurate temperature predictions [5,6]. As an extension of the previous work, we think neglecting radiative heat transfer could lead to inaccurate air flow rate in natural ventilation since buoyancy force is one of the driving forces of natural ventilation. To assess the effect of radiative heat transfer on single-sided buoyancy ventilation, computational fluid dynamics simulations of spaces are performed with and without radiative effects. It is found that ignoring radiative heat transfer will lead to inaccurate thermal stratifications, mass flow rate and surface temperatures in the room, which validates the concerns about the accuracy of the results obtained from the scale models.

4.1 Methodology

The geometry of the two-room space is remained the same as that in Chapter 3, shown in Figure 3-1. Five different cases are considered, dealing with scenarios commonly found in single-sided buoyancy-driven ventilation studies, and are summarized in Table 4-1. The same opening geometries are considered as Chapter 3: a door and a window. The height of the window from the floor is not fixed in this chapter. In case 1, a constant surface heat flux of 904.2W/m^2 (400 W in total) is generated by the heater, while the side walls of this room are modeled to be adiabatic. In the remaining cases, the heater is defined as adiabatic, while the side walls in the warm room are set at a fixed temperature of 30.0 °C. The amount of heat transferred from the walls to the air was approximately 420 W, similar (within 5%) to the heat gains due to the space heater in case 1. The temperature of the walls in the other room are kept at a low temperature of 20.0 °C

for all the cases, thereby acting as a heat sink. All other surfaces, the ceilings, floors and connecting walls, are modeled as adiabatic for all five cases.

Each case is simulated twice, with and without radiation. The air in the space is modeled using the ideal gas model and the Boussinesq approximation, giving similar results. Only the ideal gas results are included in this paper. Contour plots of temperature are shown at the location of the middle measurement plane. Plots of temperature against height are shown at the locations of the other measurement planes, one in the warm room and one in the cold one. Temperatures are expressed as excess temperatures above 20.0 °C, the lowest temperature in the space. Thus a temperature of 21.0 °C is expressed as 1.0 °C. Bulk temperature in each room is calculated by averaging, spatially, the temperature of the air in the room. In addition, the air mass flowrate is measured at the opening connecting both rooms, the flowrate given is for the air that entered one of the rooms. Mass conservation requires the amount of air that leaved the room to be the same, so the net airflow rate through the opening is zero.

Table 4-1. Summary of cases considered for the two-room space.

Case	Heat source	Opening type	Opening centerline height
1	Heater	Door	0.99 m
2	Heated walls	Door	0.99 m
3	Heated walls	Low window	0.45 m
4	Heated walls	Middle window	1.14 m
5	Heated walls	High window	1.83 m

4.2 Results

4.2.1 Effect of heat source. Cases 1: space heater, and case 2: heated walls

Figure 4-1 shows the contour plots of excess temperature for case 1 and case 2, while Figure 4-2 shows plots of excess temperature against dimensionless height (normalized by the height of the room), including and neglecting radiation. For the case with the space heater on, the temperature profile of the air is colder, by approximately 1 to 2 °C, in the lower part of the room when radiation is ignored than when including it. The excess temperature of the air near the floor is practically 0 °C in both the warm and cold room with no radiation. However, when radiation is accounted for, the excess temperature of the air near the floor was roughly 1 to 4 °C. This can also be seen as a thicker cold (blue) layer above the floor in Figure 4-1.

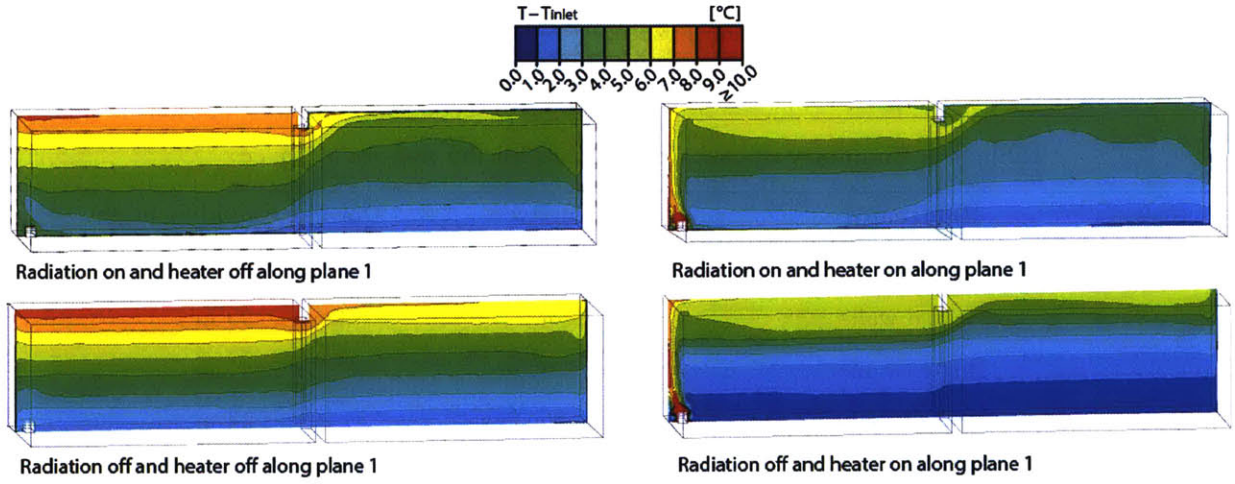

Figure 4-1. Contour plots of excess temperature for case 1 and case 2, when accounting for radiation (top) and when neglecting radiation (bottom), case1 (right) and case2 (left). Excess temperatures above 10 °C are shown in red.

For case 1 with no radiation, the excess temperature near and at the ceiling in the cold room varies from a value of 5 °C to a value of 1 °C. This variation is found to be a consequence of radiation heat transfer from the ceiling to the cold walls. The warmer temperatures seen near this area are related to the warm air from the room with the heater, while the colder temperatures are due to radiative transfer to the cold walls, thereby accounting for the greater variability in

temperatures observed here. This variability is absent in the simulation that did not include radiation, because there is no efficient way to exchange heat between the ceiling and the walls. In the warm room a similar variability in the temperature of the air is seen near and at the floor when including radiation. The floor of the warm room receive cold air from the other room, but it is also heated via radiation, either from the other walls and the ceiling, or directly from the space heater. With no radiation, the temperature near the floor stays close to the temperature of the walls of the cold room, even near the space heater. Similar temperature variability is seen near the ceiling of the cold room and near the floor of the warm room in case 2, when accounting for radiation. Except for these areas, the temperature profiles of the simulations with and without radiation are very similar in case 2, as shown in Figure 4-2.

Table 4-1 gives the bulk temperatures, T_{cold} and T_{warm}, bulk temperature differences, ΔT, and mass flowrates, $\dot{m}$, for both cases. For each case, the bulk temperatures are not considerably different when comparing the simulations with and without radiation. Neglecting radiation results in a deviation between 0.8% (case 2, cold room) and 5.6% (case 1, warm zone) in the bulk temperatures in each zone. Furthermore, ignoring radiation results in an underestimation of the air mass flowrate exchange through the opening of 31.2% for both cases.

It should also be noted that for Case 2 the mass flow rate is smaller for the case with radiation although its zonal temperature is smaller than that without radiation. This is attributed to the fact that the local temperature difference is different from the zonal temperature difference, as is introduced in Chapter 3. Although the zonal temperature difference is smaller for the case with radiation, the local temperature difference is higher, which result in larger ventilation rate.

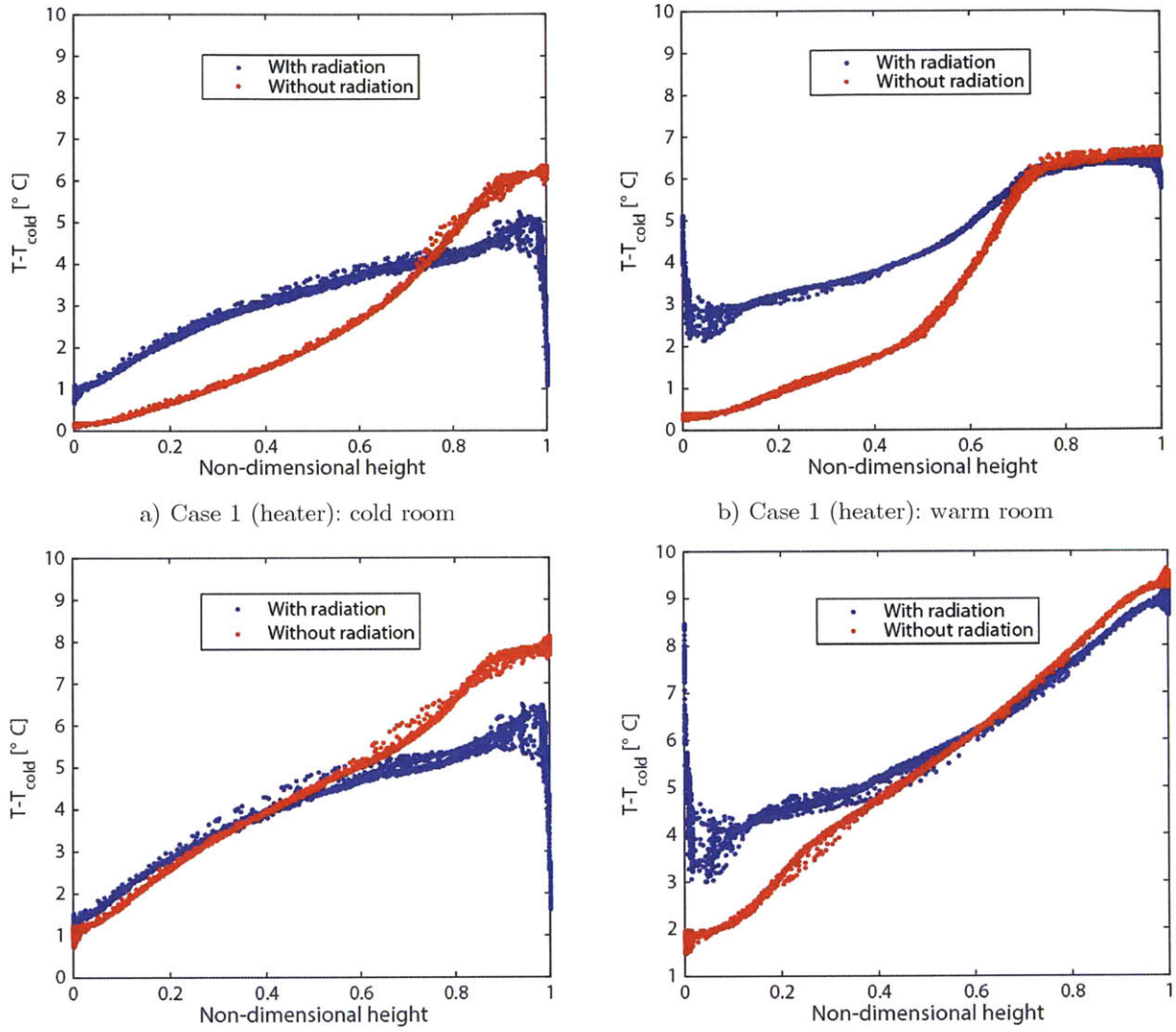

a) Case 1 (heater): cold room

b) Case 1 (heater): warm room

c) Case 2 (heated wall): cold room

d) Case 2 (heated wall): warm room

Figure 4-2. Vertical distribution of excess temperature along two measuring planes in cold (left) and warm (right) zones in cases 1 and 2.

Table 4-1. Simulation results for cases 1 and 2 with and without radiation.

Case	Radiation	T_{cold} [°C]	T_{warm} [°C]	$\Delta T = T_{warm} - T_{cold}$ [°C]	$\dot{m}$ [kg/s]
1	With radiation	22.9	25.1	2.2	0.109
(Heater)	Without radiation	22.7	23.7	1.0	0.075
2	With radiation	24.6	25.5	0.9	0.125
(Heated wall)	Without radiation	24.4	26.0	1.6	0.086

4.3.2 Effect of the vertical location of the opening. Case 3: 0.45 m, case 4: 1.14 m, and case 5: 1.83 m from the floor.

The effect of the vertical location of the opening is analyzed by moving the window vertically from floor to ceiling, while maintaining the same opening geometry and horizontal location. Three cases (case 3—5) are compared: low, middle and high window. Figure 4-3 shows the contour plots of excess temperature for these three cases, both with and without radiation. For all these cases, the heat gains are incorporated by setting the temperature of the walls in the warm room.

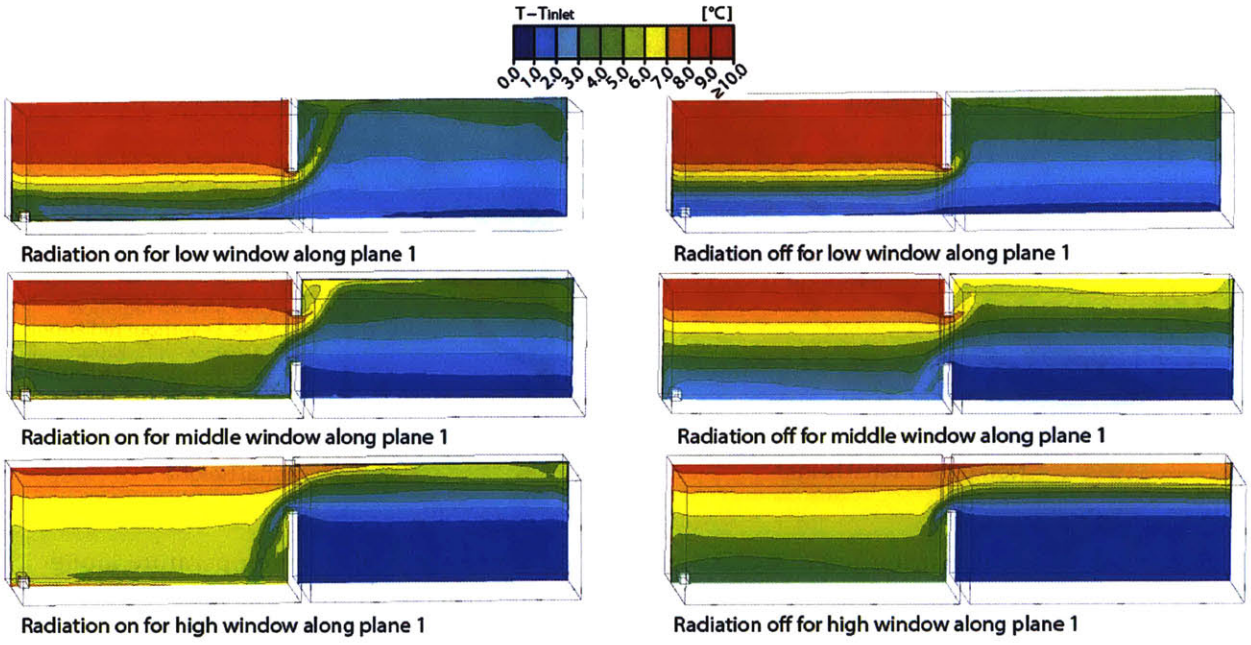

Figure 4-3. Contour plots of excess temperature for case 4 (low window), case 5 (middle window) and case 6 (high window), when accounting for radiation (left) and when neglecting radiation (right). Excess temperatures above 10 °C are shown in red.

Figure 4-4 demonstrates how vertical height of the opening affects thermal stratification patterns in the two rooms. When the opening is located near the floor, a thick layer of hot air forms near the ceiling in the warm room. When the opening is located near the ceiling, though, a thick cold layer forms near the floor of the cold room instead. In the cold room (Figure 4-4a) the temperature of the air near the ceiling increased as the height of the opening increased, because the air from the warm room is in contact with cold air in the other room for a smaller amount of

time as it makes its way from the opening to the ceiling of the cold room. Analogously, the temperature of the floor in the warm room increases with increasing height. In the cold room, the temperature of the ceiling is always lower when including radiation than when neglecting it, by approximately more than 5 °C. The temperature of the floor is, however, within 1 °C for all cases, with and without radiation. Similarly, the temperature of the floor in the warm zone is higher when including radiation, but the temperature of the ceiling is approximately the same.

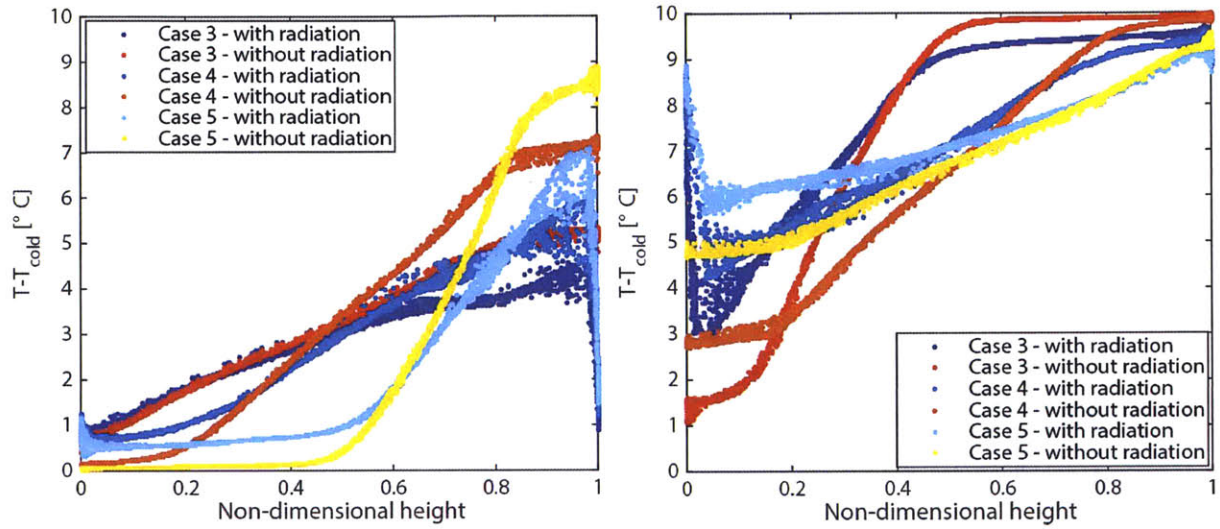

Figure 4-4. Vertical distribution of excess temperature above the cold zone temperature along two planes in a) the cold and b) the warm rooms in cases 3 – 5.

Table 4-2 gives the bulk temperatures, bulk temperature differences and mass flowrates for both cases. As in the previous two cases, 1 and 2, the simulation results with radiation consistently give higher mass flowrates. The simulation of case 4, with the opening in the middle of the height of the room, has a mass flowrate of 0.056 kg/s without radiation and 0.067 kg/s with radiation, with a relative difference of 15.8%. However, as the vertical height is changed so the opening was closer to the ceiling or the floor, this difference in the mass flowrates increases to around 26.0%. Indeed, the middle opening case shows the closest temperature contours and ventilation performance between the simulations with and without radiation.

Table 4-2. Simulation results for case 3—5 with and without radiation.

Case	Radiation	T_{cold} [°C]	T_{warm} [°C]	$\Delta T = T_{warm} - T_{cold}$ [°C]	$\dot{m}$ [kg/s]
3	With radiation	22.6	28.0	5.4	0.063
	Without radiation	23.1	27.4	4.3	0.047
4	With radiation	22.8	27.8	5.0	0.067
	Without radiation	23.5	27.2	3.7	0.056
5	With radiation	22.3	27.9	5.6	0.057
	Without radiation	22.9	27.4	4.5	0.042

4.3.3 Effect of the opening size.

Figure 4-5 shows the excess temperature profile across the middle measuring plane parallel to the opening in both cold zone and warm zone for large (door, case 2) and small (window, case 4) openings. Contour plots of excess temperatures of both cases can be found in Figure 4-1 and Figure 4-3. These two openings have similar middle-plane heights around 1.0 m, thus the vertical height of the opening can be considered to be the same. As is mentioned, including radiation leads the ceiling and floor to establish closer temperatures that flattens the temperature profiles across the entire height of each zone. It seems that by decreasing the size of the opening, the average temperature of the cold zone will become smaller while that of the warm zone will become larger. The window case has a larger integrated temperature difference between the two measuring plane in each zone than the door case. This is mainly contributed by a smaller mass flowrate which is responsible for less mixing and more zonal temperature variation.

The surface temperatures for case 4 also differ between the two radiation modes. Similar to the case 2, all surfaces vary within 2.0 °C from side wall temperatures when radiation is turned on. Nevertheless, a difference of more than 7.0 °C is developed for both cold and warm zone when radiation is neglected. Case 4 gives a mass flowrate of 0.067 kg/s for with radiation and 0.056

kg/s for without radiation, corresponding to zonal (bulk) temperature differences of 5.0 °C and 3.7 °C respectively. The mass flowrate decreases at a rate of less than a factor of 2 when the size of the opening is halved.

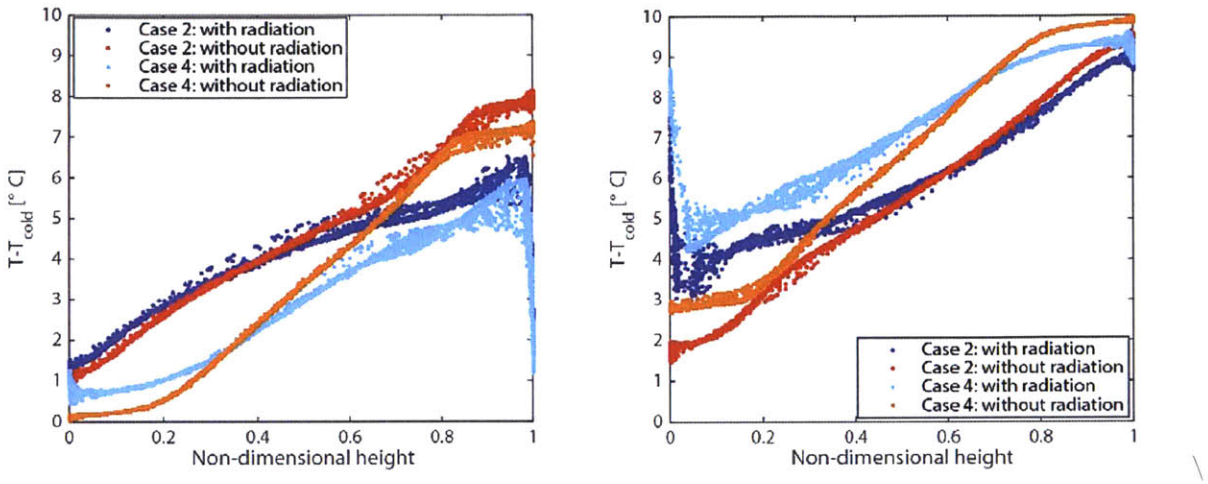

a) b)

Figure 4-5. Vertical distribution of excess temperature above the cold zone temperature along two planes warm zone, and cold zone located at the middle of each zone in case 1 (a. cold zone, b. warm zone), when radiation is accounted for (blue) and neglected (red). The excess temperature of the floor and the ceiling at these locations are also indicated in the figure.

4.4 Discussions

For all the cases explored, the simulations including radiation result in larger mass flowrates through the opening than when neglecting its effects, shown in Figure 4-5. For both opening geometries, door and window, there is a significant difference of around 31% between the results that included radiation and those that did not. Differences also exist between the mass flowrates obtained with and without radiation for cases 3 to 5, where the opening height is changed. Nevertheless, the mass flowrate in case 4, with the opening at the middle of the height of the room

is similar for both simulations with and without radiation, with a difference of approximately 16%. Therefore, water scale models for two way flow, as the one considered in this work, should be used with care, taking into consideration the flowrate underestimation observed here.

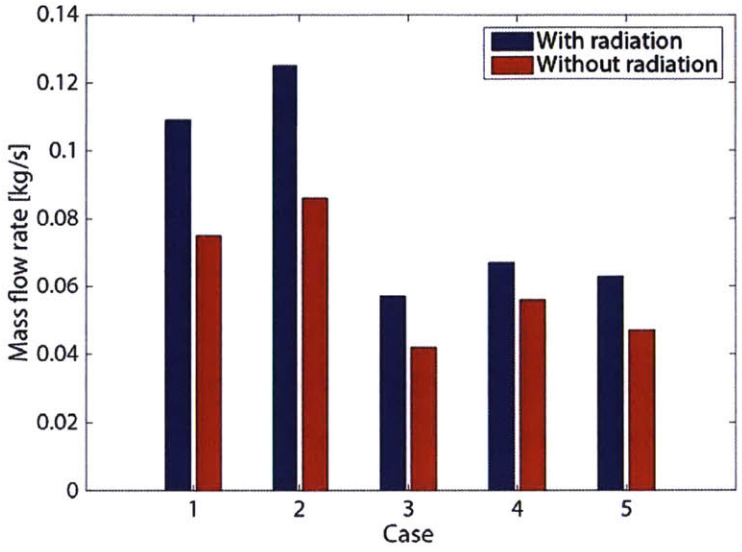

Figure 4-6. Comparison of the mass flowrates for all the different cases in the two-room space, when accounting for radiation (blue) and when neglecting it (red).

Models that neglect radiation, however, can be useful when estimating the air temperature profile in situations where the temperature of the walls is controlled, as opposed to the other situation considered here of an space heater. In this situation, the results between the simulations that included and neglected radiation are found to be similar, especially in the cold zone. The difference is small because the heat gains are distributed among some of the surfaces of the room. However, when the heat gains are concentrated, as in the space heater case, the error associated with ignoring radiation increases. Therefore, scale water models might result in an inaccurate prediction of both fluid field and mass flowrate when heat sources are concentrated spatially.

4.5 Conclusions

Accounting for radiation exchange is found to be of critical importance when studying the air flow and thermal dynamics of a space ventilated using buoyancy-driven flow. Ignoring the effects of radiation was found to cause a consistent underestimation of the mass flowrate for the two-way flow model. It is found that neglecting radiation results in unrealistic thermal stratification profiles, especially when the heat source is concentrated in a small region. Scale water models might be useful when analyzing cases with distributed heat sources or with an opening in the middle of the height of the room. Nevertheless, even in these situation, it should be considered that in the real-sized space, the temperature of the air surrounding the occupants might be approximately 2 °C higher and the mass flowrate 16% higher than predicted by the scale water model. Consequently, temperature profiles, mass flowrates, surface temperatures and any other results that depend on these variables are of limited usefulness in realistic spaces, when obtained using computational or experimental methods that ignored the effects of radiation.

5. FLOW CHARACTERIZATION OF BI-DIRECTIONAL VENTIALTION IN MULTI-ZONE WITH ASSITING WIND AND BUOYANCY FORCES

Abstract: Unidirectional and bi-directional flows are the essential patterns in natural ventilation. While unidirectional and single-sided ventilations are extensively explored, multi-zone bi-directional natural ventilation is still quite poorly understood. To investigate it, we consider the natural ventilation of a heated room connected to the cold ambient and to an atrium at the ambient temperature with fixed sidewall temperature and fixed heat flux boundary conditions, with and without wind. The transient flow behaviors are studied by computational fluid dynamics. For the windy cases the wind force overwhelms the thermal buoyancy and only unidirectional flow is observed; whereas for the windless case, the initial bi-directional flow is shown to warm up the atrium and promote the establishment of the final unidirectional pattern in the CFD simulation, whereas no ventilation occurs in the flow network model. These results confirm that neglecting bi-directional flow pattern can result in problematic steady-state solutions and unreliable estimation.

Keywords: bi-directional, single-sided, wind, natural ventilation, CFD, flow network, modeling.

5.1 Introduction

Prediction and control of natural ventilation is rather difficult due to the unsteadiness of driving forces [1,2], complexities in building geometries [3] and coupling between thermal mass and natural ventilation [4], especially for multi-zone ventilation. For simplicity, a unidirectional flow pattern in openings is typically assumed for multi-zone ventilation [5]. This is mainly because unidirectional flow is the prevailing flow mode in natural ventilation while bi-directional flow only appears in a limited number of cases such as single-sided ventilation [6] and openings neighboring the neutral plane of a building [7]; simplified models [7,8] have been established for these cases.

Studies have reported that multiple solutions can exist in unidirectional systems when the wind opposes thermal buoyancy [9,10]. Shuang Duan and Yuguo Li [11] investigated the natural ventilation through a two-opening building connected with the ambient and found that the unidirectional flow assumption led to the existence of two stable solutions for the buildings considered. Moreover, they proved that bi-directional flow could also exhibit multiple solutions under opposed wind and buoyancy forces based on their multi-zone macroscopic simulations. However, it is unclear how the flow patterns affect the natural ventilation solutions in multi-zone systems, especially when the wind assist buoyancy forces.

Meanwhile, not only the steady state solution but also the transient process is important for natural ventilation estimation. Paul Linden pointed out that the establishment for a complex real building environment can take hours [12]; instantaneous ventilation performances are of importance. Therefore, the flow behaviors of bi-directional ventilation in buildings should be carefully investigated and understood.

Therefore, this work is designed to investigate the role of bi-directional flows on the natural ventilation in a multi-zone system, where a heated room is connected with the cold ambient and an atrium at the ambient temperature with different wind velocities, using computational fluid dynamic. This geometry is a common natural ventilation scenario in buildings with a side chimney. Meanwhile, we analyze the transient flow behaviors and patterns with a goal of understanding the mechanisms of bi-directional flow under assisting wind and buoyancy forces.

5.2 Methodology

The geometry in this study contains a heated room, a cold atrium and the ambient environment. The room dimensions is based on the geometry of an experimental chamber at Massachusetts Institute of Technology [13]. The room space is 2.28 m high, 5.16 m long and 3.57 m wide. The heated room is connected with both the atrium and the ambient through two opposite openings,

shown in Figure 5-1. The openings are located in the middle of two opposite walls, each opening is a 0.90 m by 0.90 m square, locating in the center of each side wall. The atrium is 10.00 m high, 2.00 m long, and 3.57 m wide. The thickness for all of the walls in the room and the ambient zones is 0.18 m. The ambient zone is designed to be substantially larger (15.00 m high, 20.00 m long and 20.00 m wide) than the room/atrium so that it can be considered as an infinite zone. Both the room and atrium spaces are contained in the ambient zone. Two measuring planes are inserted in the model to show thermal and ventilation performances: measuring plane 1 is located in the middle of the entire domain across the room and the atrium and measuring plane 2 is located in the middle of the room parallel to the openings, shown in Figure 5-1.

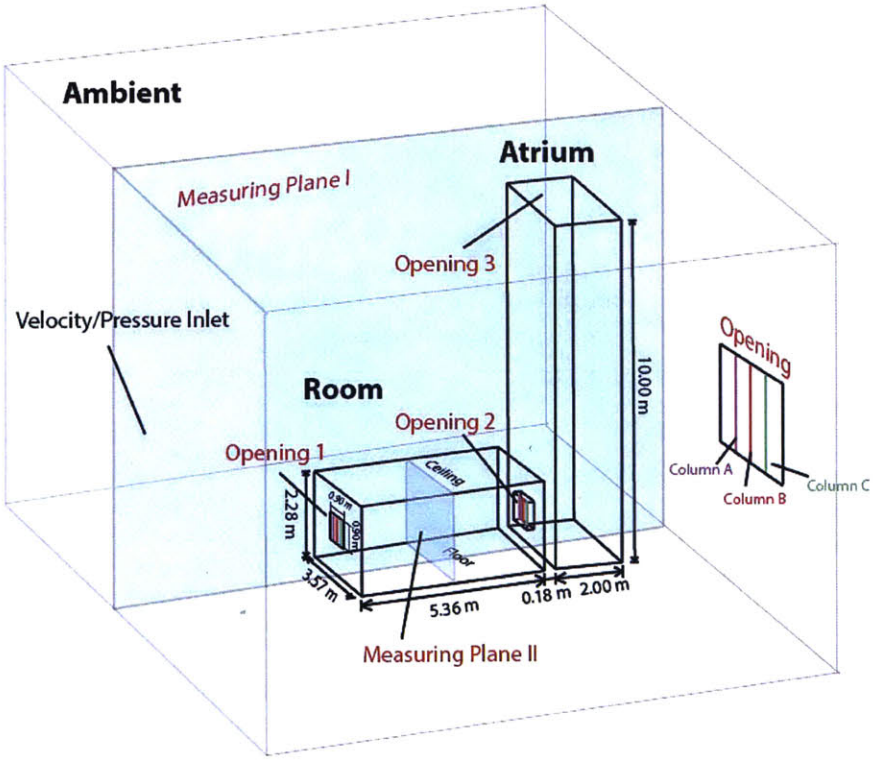

Figure 5-1. Domain of the CFD model. Four measurement planes are indicated in the figure. Two of them are parallel to the symmetry planes, and two are parallel to the inlet and outlet walls. The colored lines at each opening are the measuring lines that are named columns A, B and C. The distance between the columns is 0.30 m; the distance from Column A or C to the inner boundary of the opening is 0.15 m.

Initially, the air in the atrium and the ambient is uniformly at 20.00 °C, while that in the room is at 30.00 °C. The atrium walls (including the floor) are modeled to be adiabatic, no-slip walls. Two sets of boundary conditions are considered for the room surfaces: i) no heat source, all room surfaces are adiabatic; ii) all of the sidewalls, ceiling and floor have a constant heat flux. The first set of boundary condition approximates the condition where a warm space without a heat source is cooled down by the cold ambient air; the second sets represent a room with constant internal heat gains. A pressure-based solver is used together with the Boussinesq approximation. The ambient surface facing the room opening is modeled to be the velocity inlet with a velocity of 1.00 m/s when there is ambient wind and the pressure inlet when the ambient is windless (zero gauge pressure). The ambient floor is set to be adiabatic, no-slip boundary. The remaining surfaces are modeled to be pressure outlets at zero gauge pressure. A fixed temperature of 20.00 °C is applied to all surfaces of the environment zone so as to maintain a constant ambient temperature. Therefore, a total of four cases are simulated with computational fluid dynamics, as is summarized in Table 5-1.

Table 5-1. Summary of boundary conditions for all four cases modelled by computational fluid dynamics simulations.

<table>
<tr><th rowspan="3">Case</th><th rowspan="2">Initial conditions [°C]</th><th colspan="2">Ambient</th><th colspan="2">Room</th><th rowspan="3">Atrium</th></tr>
<tr><th rowspan="2">Velocity inlet</th><th rowspan="2">Sidewalls/ ceiling</th><th rowspan="2">Sidewalls/ Floor/Ceiling</th><th rowspan="2">Connecting wall</th></tr>
<tr><th>$T_{ambient}/T_{room}/T_{atrium}$</th></tr>
<tr><td>A</td><td rowspan="4">20.00/30.00/20.00</td><td rowspan="2">Wind velocity at 1.00 m/s; 20.00 °C</td><td rowspan="4">Zero gauge pressure, 20.00 °C</td><td>Adiabatic</td><td colspan="2" rowspan="4">Adiabatic</td></tr>
<tr><td>B</td><td>30.0 W/m²</td></tr>
<tr><td>C</td><td rowspan="2">Windless, 20.00 °C</td><td>Adiabatic</td></tr>
<tr><td>D</td><td>41.1 W/m²</td></tr>
</table>

All of the cases are simulated using Fluent (part of the ANSYS 14.5 suite). The turbulence model used is the RNG k–ϵ. This turbulence model has been shown to accurately simulate room airflow dynamics [14]. The near–wall regions are meshed using very fine elements ($y^+ \lesssim 5$), as required by the "enhanced wall treatment" used in this study [15]. The surface-to-surface model is used as the radiation model. This radiation model treats the air as being perfectly transparent

to radiation, which is a valid approximation for air with low humidity content and in spaces of relatively small dimensions [16]. The emissivity of all of the surfaces is defined to be 1. This simplification is justified given that typical materials in an office, except for polished metals, have emissivities above 0.9 [17]. The cases are run as transient simulations and stopped until a real time of 500 seconds due to limited computational ability. The thermal stratification and ventilation performance at 500 seconds are very close to the steady state simulation so that they are treated as steady state solutions. For each of the four cases, the relative errors of energy and mass conservations at each time step in the simulations are controlled within 5.0 %. The results of the CFD model used here have been validated by comparison with the experiments in the works by Nansteel and Greif [18] and Olson et al. [19].

5.3 Results and Discussion

5.3.1 Steady state solutions

As previously mentioned, each of the cases (with/without wind; with/without heat source) is modelled using computational fluid dynamics transiently until a real time of 500 seconds. Table 5-2 shows the steady state ventilation rates and thermal conditions for each case. The results at 500 seconds in the CFD simulations are used as steady state solutions due to limited computational ability; this is an approximation because the room/atrium temperatures of Case C have not reached 20.0 °C at 500 second. However, we assume this is close enough to steady state.

Since the thermal buoyancy is assisting the wind, the mass flow rate for cases with heat source is larger for the cases without heat source given the same wind velocity. In the presence of ambient wind, the case with heat source (Case B) gives a 34.1 % higher mass flow rate than that without heat source (Case A); when the ambient is windless, with heat source (Case D) gives a 66.7% higher mass flow rate than without heat source (Case C). Meanwhile, thermal stratification

between the room and the atrium for the cases with heater is observed as the room temperature is higher than the atrium temperature at steady state.

These results are unexpected because conventional network model assuming unidirectional flow gives completely different steady state solutions for some of the above-mentioned cases. For instance, there will not be any ventilation because the ambient and the atrium are initially at the same temperature in a windless environment and there is no pressure gradient between the atrium and the ambient. That is to say, the air in the room will be stationary and constantly being heated by the indoor heat source. Therefore, over certain period of time, the room temperature will be extremely high yet the atrium is still remained at the initial temperature due to the lack of ventilation. The steady state solutions from CFD suggest that the flow patterns are by no means unidirectional throughout the 500 seconds of simulation.

Table 5-2. Simulation results of the solutions at 500 seconds of the all of models from CFD models.

Case		Numerical methods	Ventilation rate (net flow rate) [m^3/s]	T_{room} [°C]	T_{atrium} [°C]
Windy, without heat source	A	CFD	0.44	20.0	20.0
Windy, with heat source	B	CFD	0.59	23.6	21.2
Windless, without heat source	C	CFD	0.15	21.0	20.5
Windless, with heat source	D	CFD	0.25	25.2	21.1

5.3.2 Transient flow behaviors

5.3.2.1 Windy cases

To understand the flow development, Figure 5-2 gives the contour plots of the excess temperatures and velocity stratifications in the CFD cases with a wind velocity of 1.00 m/s with and without internal heat gains (cases A and B) at different times (t = 10, 25, 100, 250 and 500 s) along measuring planes 1 and 2. From the simulation results, no two-way flow pattern is observed for the windy cases throughout the entire flow development processes.

Initially (t = 10 s), the wind pressure in the ambient causes a pressure gradient between the ambient and the room; a downward cold jet occurs at opening 1 and enters the room, mixing with the warm air in the room. As the room is gradually cooled down by ambient air (t = 25 s), the buoyancy resistance decreases and the downward jet pattern starts to redirection. Meanwhile, as the temperature of the room decreases, the buoyant resistance decreases and the velocity of the jet increases. As the flow develops (t = 250 s), a high momentum mainstream air flow though passes through opening 1 and 2, which is very similar to pipe flow, shown in measuring plane 2 temperature contours. A vertically symmetric thermal stratification forms and the fingering pattern becomes almost horizontal. The atrium temperature gradually reaches the air temperature from opening 2. At final simulation stage (t = 500 s), the temperatures of each zone reach relative stable values and thermal stratification in each zone start to establish.

It should be noted that although the wind force and the buoyant force are assisting each other for the ventilation through opening 2 to opening 3, the high room air temperature tends to resist the ambient air from entering through opening 1 due to thermal plumes. This local thermal resistance will affect the velocity profiles at the openings; this will be discussed in Section 5.3.4.

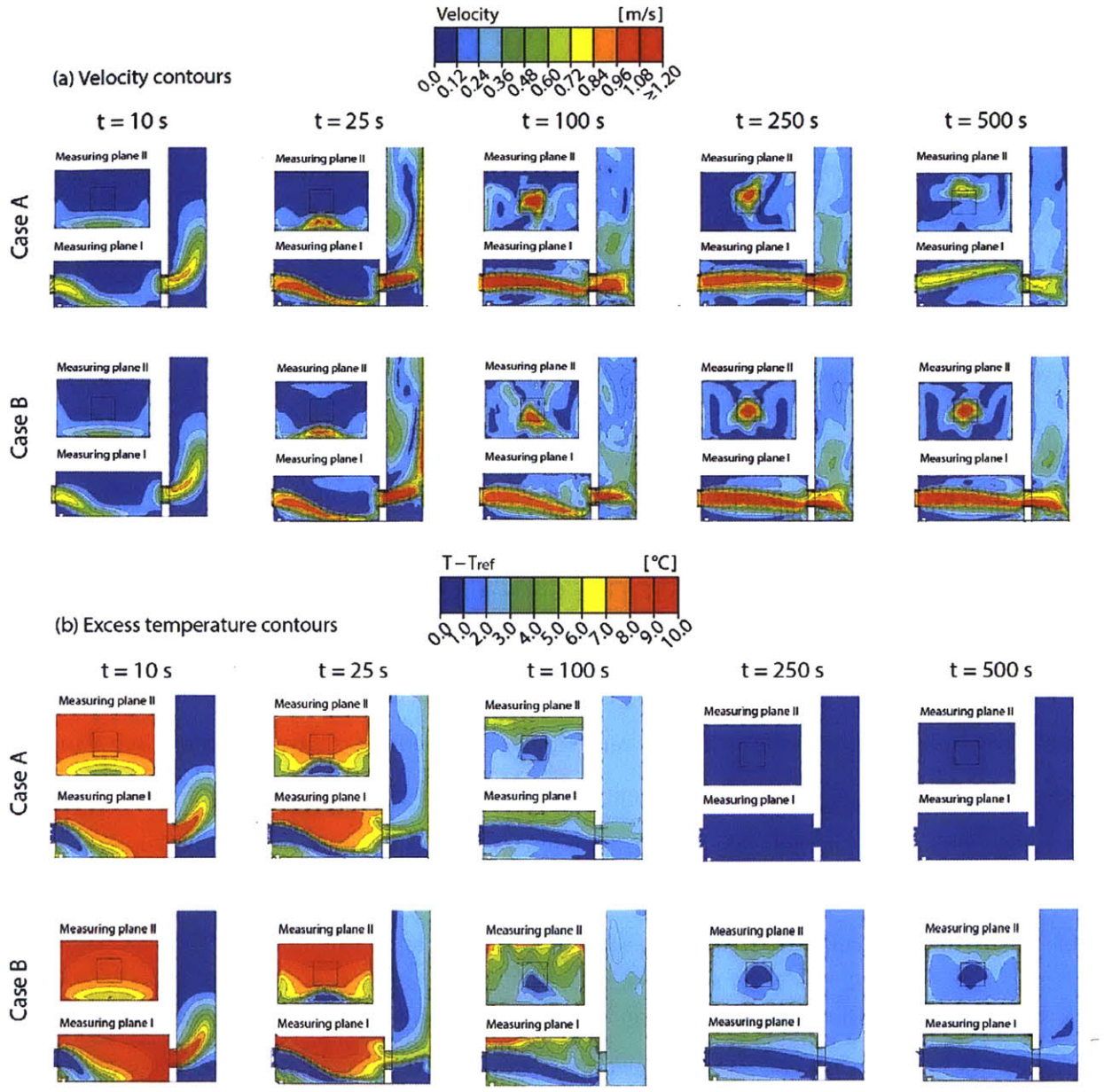

Figure 5-2. Contour plots of velocity profiles (a) and excess temperatures (b) of the CFD simulations of cases A and B with a velocity of 1.00 m/s at t = 10, 25, 100, 250 and 500 s. The flow pattern at the top of the chimney is not of interest and thus not shown in the figures.

5.3.3.2 Windless cases

Similar to the windy cases, Figure 5-3 gives the contour plots of the excess temperatures and velocity stratifications in the CFD cases of the windless cases with and without internal heat gains (cases C and D) at different times (t = 10, 25, 100, 250 and 500 s) along the two measuring planes. A transition from bi-directional airflow to unidirectional airflow is observed in the windless cases.

As is mentioned in 5.3.3.1, the local thermal resistance due to the plume effect tends to resist ambient air from entering the room, resulting in bi-directional flow at opening 1. Initially the atrium and the ambient is at the same pressure and no unidirectional flow is observed. Pure bi-directional single-sided buoyancy-driven ventilation (at a low velocity) is established at both sides due to the temperature difference between room/ambient and room/atrium at the initial stage (t $<$ 10 s). As the atrium is gradually heated by air from the warm zone (t $<$ 25 s), a horizontal pressure gradient starts to establish. Bi-directional pattern still remains its form, however the net flow rate into the room from the ambient at opening 1 as well as that into the atrium from the room at opening 2 starts to increase. Between t = 100 s and 250 s, the flow evolves into unidirectional.

It should also be noted that the time that the bi-directional pattern disappear at each openings is different: the bi-directional airflow pattern first disappears at opening 2 and then opening 1. This is due to the dynamic changes in zonal temperature as well as zonal pressure, which will be discussed in Chapter 6. A long plume jet is observed at opening 2. However, as the room temperature decreases and stabilizes, the jet becomes a short local thermal dissipation at the opening. At final simulation stage (t = 500 s), the thermal stratification pattern is more similar to single-sided buoyancy ventilation in the presence of layered stratification because the ventilation is still buoyancy-induced despite of the unidirectional air flow pattern.

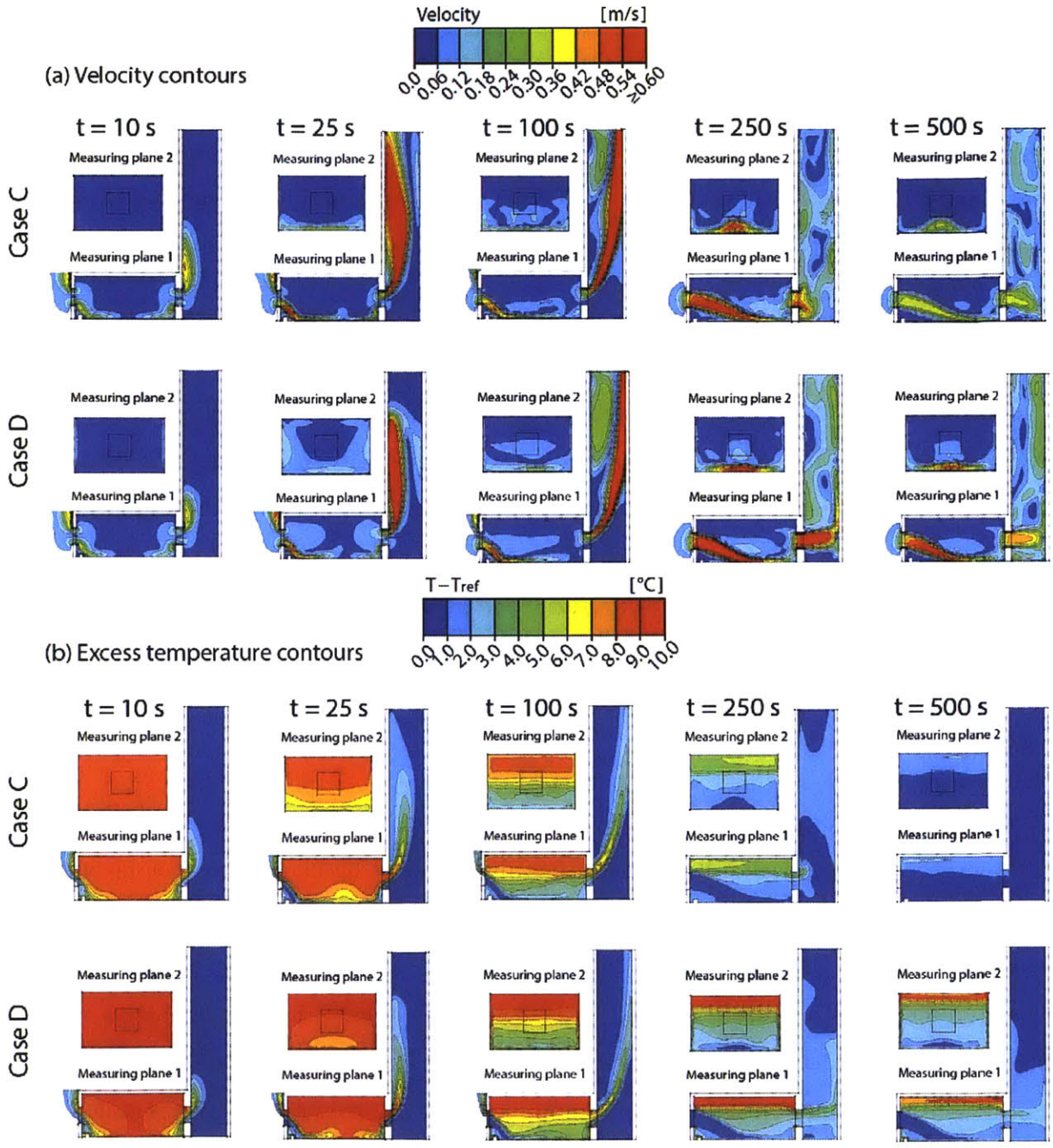

Figure 5-3. Contour plots of velocity profiles (a) and excess temperatures (b) of the CFD simulations of windless cases C and D at t = 10, 25, 100, 250 and 500 s.

5.3.3 Velocity profile at the openings

5.3.3.1 Windy cases

Figure 5-4 plots the velocity profiles across columns A, B and C in Figure 5-1 for cases with ambient wind (cases A and B). As previously mentioned, the flow pattern remains unidirectional throughout the whole ventilation process (0 s $<$ t $<$500 s). The velocity profiles at the openings are not uniform: the air at the core of the stream exhibits higher velocities while that near the boundaries exhibits lower velocities.

For the case without heat source (Case A), the maximum air velocity in the 500 seconds is roughly at 1.0 m/s, which is the ambient wind velocity. In the initial ventilation stage (t = 10 s), the air velocity at opening 1 is small (about 0.6 m/s) due to the large buoyant resistance. As the ventilation cools the air in the room, the buoyancy resistance becomes smaller and the velocity of the jet at opening 1 increases to almost 1.0 m/s. This increase is caused by the combination of the ambient wind as well as the stack effect. However, when the room air temperature decreases to a certain value, the stack effect diminishes and the wind force is dominating. The jet velocity will eventually stabilize at a constant value when the room air reaches the ambient temperature.

For the case with heat source (Case B), the air velocity is relatively higher than the adiabatic case and the maximum air velocity can be as high as 1.5 m/s. This is contributed to by the increased stack effect from the heat supply. Even at the steady state, the room will still remain at a higher temperature than the ambient thanks to the internal heat gains.

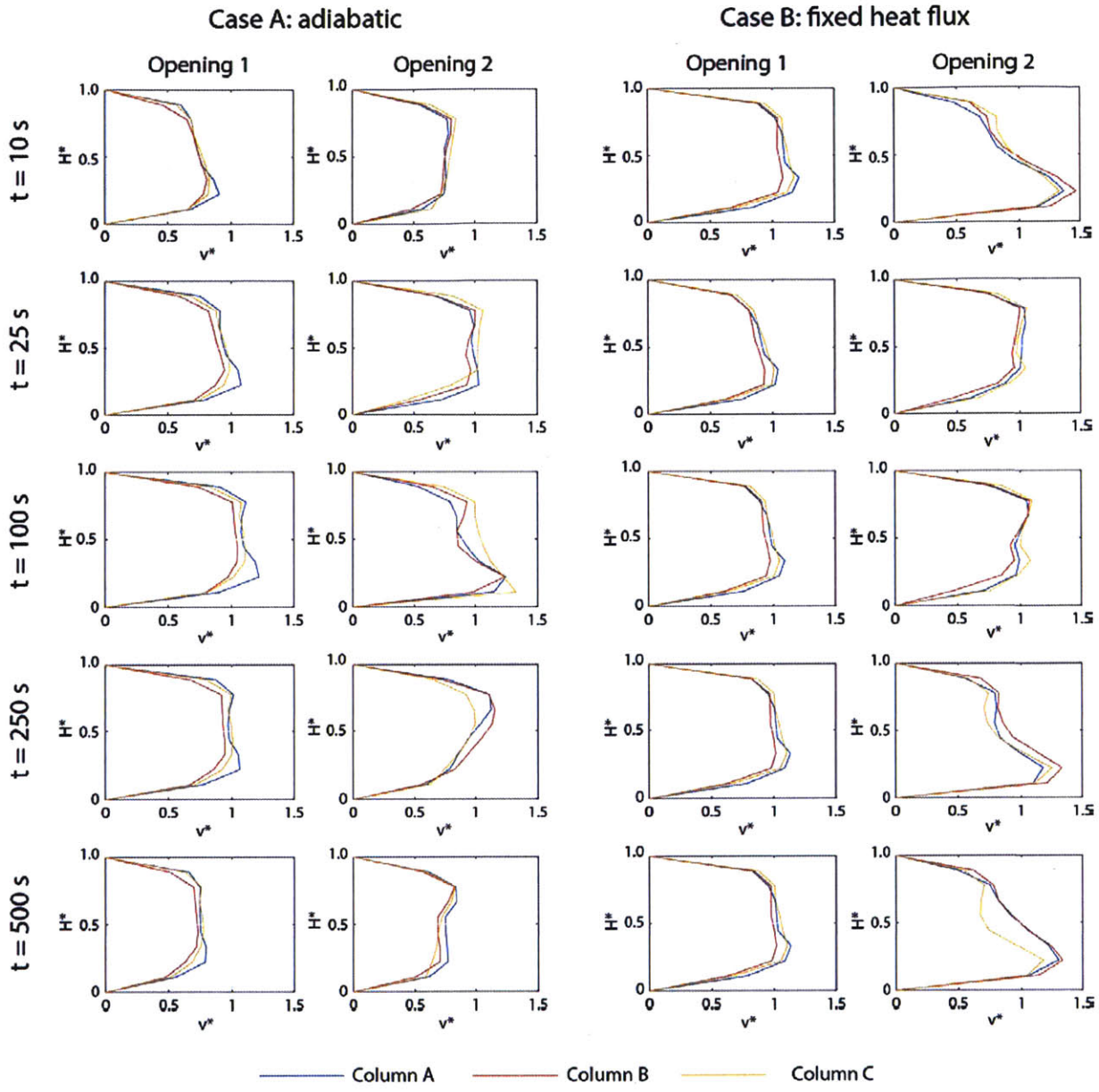

Figure 5-4. Velocity profiles of the CFD simulations of cases A and B with a velocity of 1.00 m/s at openings 1 and 2 at t = 10, 25, 100, 250 and 500 s. H* is the non-dimensional height, which is defined by the ratio of actual height above the bottom of window and the opening height (0.90 m).

5.3.3.2 Windless cases

Similarly, Figure 5-5 plots the velocity profiles across columns A, B and C in Figure 5-1 for the windless cases (cases C and D). The transition from bi-directional airflow to unidirectional airflow is observed at both openings 1 and 2.

It is interesting to notice that the bi-directional flow patterns at the two openings (1 & 2) are symmetric, as is shown in Figure 5-5. Initially, the room is of a higher temperature such that the room air exits from the upper parts of both openings 1 and 2. As the flow develops, the atrium is slightly warmed up and it forms a pressure gradient between the ambient and the atrium; the velocity profiles at both openings moves in the direction of x-axis in Figure 5-5. More ambient air enters the room and less room air escapes to the ambient. Due to mass balance, the excess air from the ambient forces more room air into the atrium. The pressure gradient becomes larger as the atrium is further warmed up by the room air and the flow becomes completely unidirectional.

Meanwhile, the atrium temperature will eventually be the same as the room temperature as the room is gradually cooled down by ambient air. For the case without heat source (Case C), the room and atrium temperatures will eventually become the ambient temperature. When it reaches steady state, no ventilating will occur due to the lack of thermal buoyancy. On the other hand, for the case with heat source (Case D), the atrium temperature will stabilize at a relatively constant value, so does the pressure gradient. Therefore, the mass flow rate will remain constant at steady state. This is observed as the velocity profiles in Case D at t = 250 s are almost the same as those at t = 500 s. The instantaneous thermal and ventilation performances will be discussed in the following section.

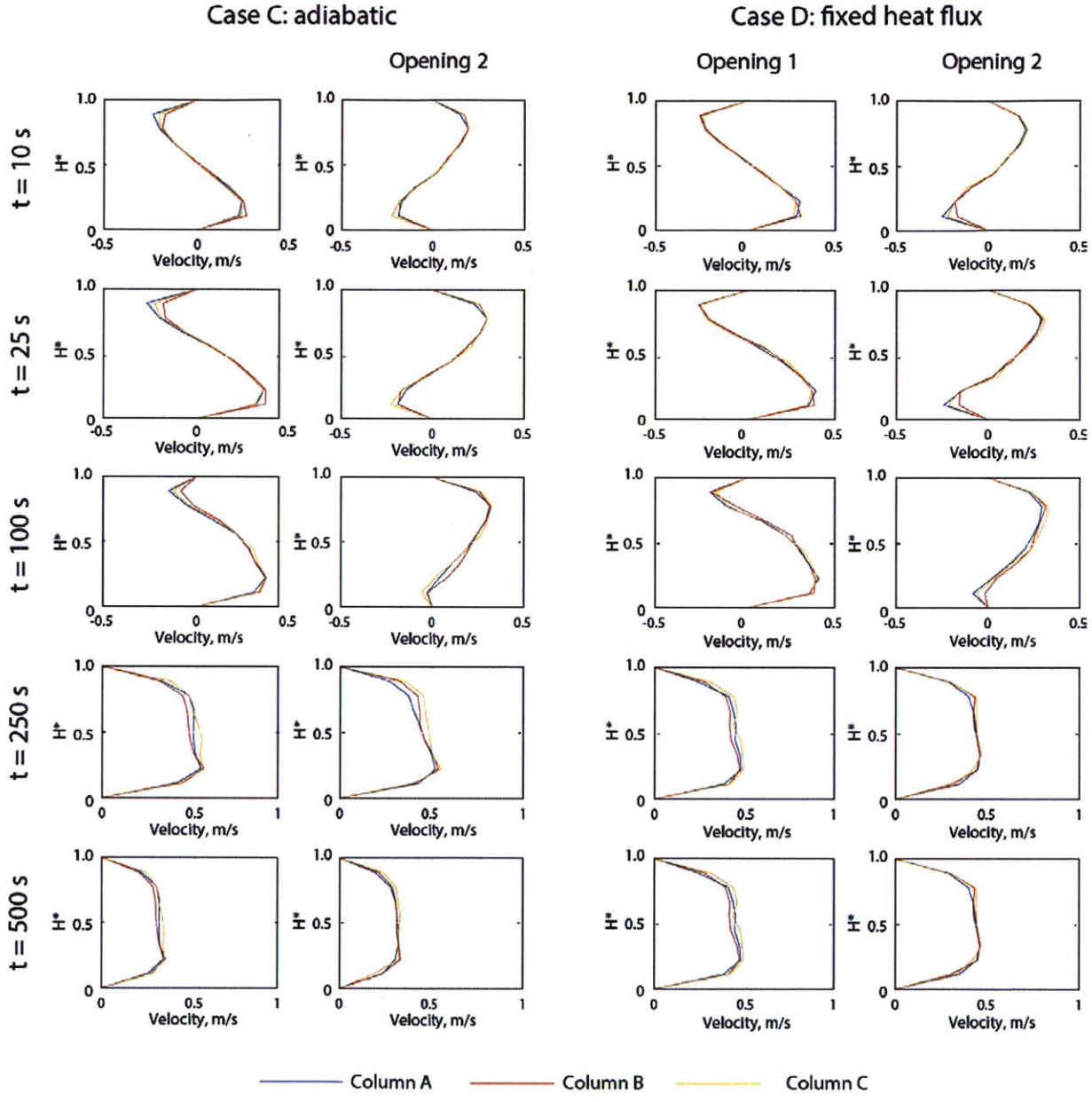

Figure 5-5. Velocity profiles of the CFD simulations of windless cases C and D at openings 1 and 2 at t = 10, 25, 100, 250 and 500 s. H* is the non-dimensional height, which is defined by the ratio of actual height above the bottom of window and the opening height (0.90 m).

5.4 Thermal and ventilation performance

Figure 5-6 gives the instant mass flow rate and zonal temperatures for the room and the atrium over 500 seconds for cases A, B, C, and D. The mass flow rate is measured as the net flow rate through any of the three openings (the net mass flow rates are the same because of mass conservation). The zonal temperatures are calculated as the averages of the temperatures of all the nodes in the room and the atrium in the CFD simulations.

As is shown in the figure, the ventilation performances for the windy cases is substantially better than the windless cases. The mass flow rates for the windy cases at t = 500 s are around 0.60 kg/s while those for the windless cases are only around 0.25 kg/s. It is also noted that it is faster for the windy cases to reach steady state than the windless cases. In Figure 5-6a, the mass flow rates for the windy cases increase steadily in the first 100 seconds and start to stabilize at relatively constant values; the zonal temperatures stabilize at around 200 seconds after the ventilation starts. However, the trend without wind in the mass flow rate is non-steady throughout the whole 500 seconds and the zonal temperatures are still decreasing at t = 500 s. This disparity between the windy and windless cases might be stemmed from the fact that the flow patterns in the two scenarios are essentially different: the flow pattern is always unidirectional in the windy cases, whereas the flow transits from bi-directional to unidirectional in the windless cases.

Meanwhile, the results also suggest that heat source has more impact on the zonal temperatures than the mass flow rate. For example, the zonal temperature difference between the room and the atrium in Case D at 500 s is approximately 4.2 °C, whereas that in Case C is about 0.5 °C; the mass flow rate for Case D is 0.3 kg/s and that of Case C is 0.2 kg/s. The temperature difference between the ambient and the atrium is an indicator of the mass flow rate because the "natural convection" model (Equation 3-1) gives a correlation between the mass flow rate and the square root of the temperature difference between the atrium and the ambient. This is validated by the simulation as at 500 s, the temperature difference is around 1.0 °C for Case D and 0.5 °C for Case C, and the ratio of their mass flow rate is roughly 1.45.

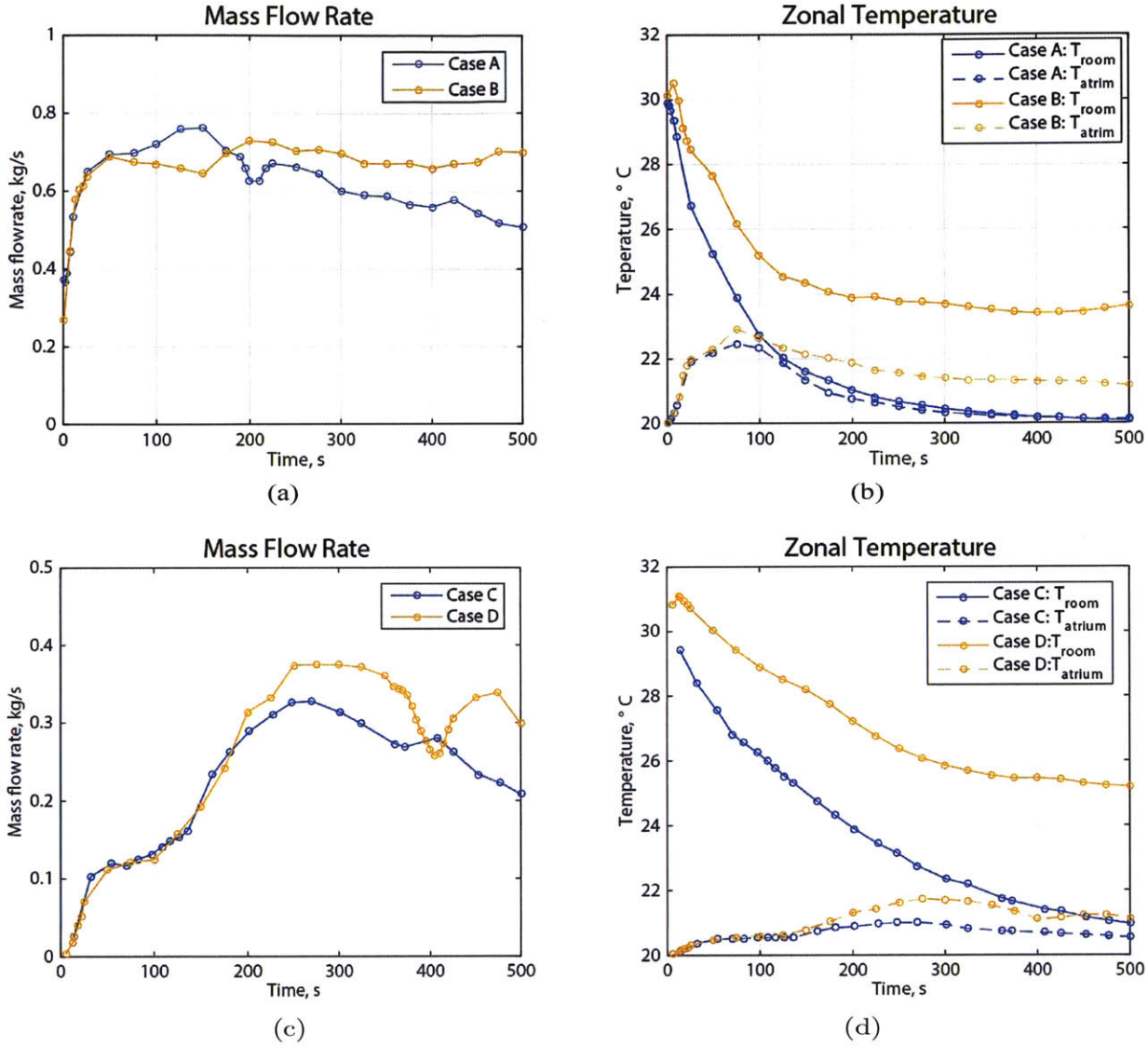

Figure 5-6. Change of mass flow rate and spatially averaged room/atrium temperature over 500 s for windy cases (upper, cases A and B) and windless cases (bottom, cases C and D) with (yellow) and without (blue) heat source.

5.5 Conclusions

In this chapter, we study the transient behaviors of air flow in a geometry where a heated room is connected with the ambient and a cold atrium through two opposite openings, with and without ambient wind, using computational fluid dynamics. Analysis of the transient flow behaviors as well as the steady state solutions are performed to both the windy and windless cases.

In the windless cases, the CFD simulations suggest that bi-directional flow occurs during the initial stage at both openings 1 and 2 that warms up the atrium and causes a pressure difference between the ambient and the atrium, resulting in unidirectional flow at steady states. In the windy cases, the flow pattern in the CFD simulations throughout the whole process was unidirectional because the initial net flow is non-zero in the presence of wind pressure. The results suggest that initial bi-directional flow pattern will affect the steady state solutions; neglecting bi-directional flow in natural ventilation will result in inaccurate estimations and problematic solutions of natural ventilation, casting doubt to the unidirectional flow assumption that is often made in conventional flow network models.

6. PREDICTION OF TRANSIENT BI-DIRECTIONAL NATURAL VENTILATION

Abstract: Bi-directional flow is an essential but poorly understood scenario in natural ventilation because it is strongly related with instantaneous thermodynamics conditions [1]. Neglecting the bi-directional airflow will result in multiple or problematic solutions [2]. However, understanding and predicting the bi-directional natural ventilation is challenging due to the complexities in the changing airflow pattern and the strong coupling between ventilation and temperature. In this work, we characterize the flow features and develop a physical model for predicting the bi-directional airflow under combined wind and buoyancy forces and validate it through CFD simulation. This model is shown to be able to simulate the thermal and ventilation performances, the time-dependent neutral plane height as well as the transitional airflow patterns. This work provides insights into the role of bi-directional flow in determining the steady state solutions of ventilation and thermal performances and offers important fast prediction tools for design purposes.

***Keywords*:** bi-directional airflow, buoyancy, wind, discharge coefficient, neutral plane height, natural ventilation.

6.1 Introduction

The concerns about energy consumption in buildings due to the dwindling fossil fuel supply [3,4] as well as the environmental impact, in terms of pollution [4] and climate change [5], have promoted serious consideration of natural ventilation. It is critical to understand the flow pattern to improve the reliability of natural ventilation to satisfy indoor air quality [6,7] and thermal comfort [8,9] in buildings. Bi-directional airflow is one of the essential but poorly understood scenarios in natural ventilation where the temperature gradients drive the air to exchange in bi-directional or multi-directional form.

Single-sided buoyancy-driven natural ventilation, where two zones of different thermal conditions are connected with a single opening, is the simplest bi-directional airflow with an established physical model – the "natural convection" model [10]. This model relates ventilation rate with stack pressure for plain rectangular openings by using Bernoulli's principle and the discharge coefficient, a non-dimensional parameter characterizing the ratio of real mass flowrate and ideal mass flowrate. However, this model only couples temperature with ventilation at a certain time but fails to predict the transitional flow development. In fact, the establishment of steady state for a complex real building environment can take hours [11] and instantaneous ventilation performances are of importance.

As for buildings with multiple openings, existing models simplify the flow network by assuming unidirectional airflow for buildings, for mathematical simplicity. Shuangping Duan and Yuguo Li [2] pointed out that the assumption of unidirectional flow has indeed led to the existence of multiple or problematic solutions for some testing buildings. For example, for a warm room with two openings, a high one for the ambient and a low one for an unheated atrium that started at ambient temperature, unidirectional flow assumption can indicate that warm air from the room never enters the atrium. Therefore, a multi-physics model, which associates the flow pattern with instantaneous thermodynamics conditions, is needed to accurately predict and control natural ventilation, especially for openings with relative large heights.

In this chapter, we develop a numerical model for predicting the thermal and ventilation performance, as well as neutral plane height for both single-opening and multi-opening systems based on the CFD simulation results in the previous chapters. The nondimensional model is shown to be able to accurately predict the instantaneous zonal averaged temperature, ventilation rate, neutral plane height and transition of airflow patterns by conservation of momentum, mass, and energy.

6.2 Model generalization

In this chapter, four cases are considered from the two geometries based on the models considered in the previous chapters i). Case 1 (Figure 6-1a): room-room model; ii). Case b (Figure 6-1b): room-ambient model; iii).Case 3 (Figure 6-1c): three-zone model with windy ambient; iv). Case 4 (Figure 6-1c): three-zone model with windless ambient. Only fixed temperature conditions are considered for side walls for cases 1 and 2, while two different boundary conditions (adiabatic, and fixed heat flux) are considered for the side walls for cases 3 & 4. Figure 6-2 shows the transient thermal and velocity stratification for each of the four cases. Part of the results has been demonstrated in previous chapters. All the cases are run transiently in CFD simulations. The detailed information of each case is listed in Table 6-1.

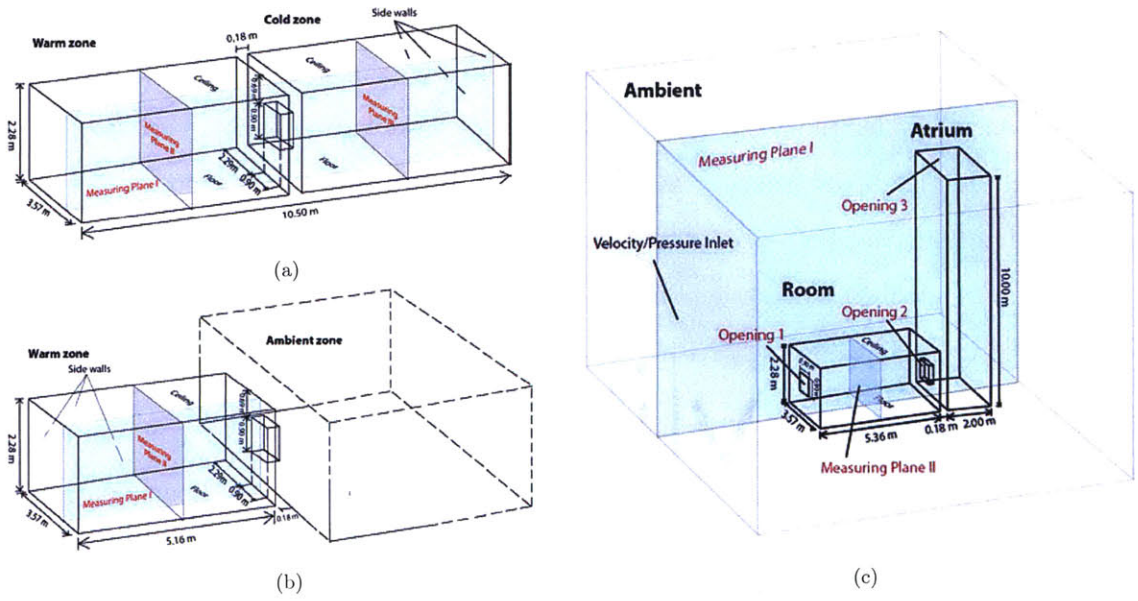

Figure 6-1. Schematic of models analyzed in this paper (a. room-room model; b. room-ambient model; c. multi-zone model with an atrium)

Table 6-1. Summary of boundary and initial conditions for the four cases. a). Two zone model, b). Three zone model.

(a)

Two zone model	Boundary conditions				Initial conditions	
	Warm zone		Cold zone		T_{warm} [$^{\circ}C$]	T_{cold} [$^{\circ}C$]
	Side walls [$^{\circ}C$]	Others	Side walls [$^{\circ}C$]	Others		
Case 1: room-room	30	Adiabatic	20	Adiabatic	30	20
Case 2: room-ambient			20 $^{\circ}C$ air temperature			

(b)

Three zone model	Boundary conditions						Initial conditions		
	Room (warm)		Ambient (cold)			Atrium	T_{room} [$^{\circ}C$]	T_{atrium} [$^{\circ}C$]	$T_{ambient}$ [$^{\circ}C$]
	Side walls	Others	Pressure/ velocity inlet	Floor	Others				
Case 3	Adiabatic	Adiabatic	Velocity inlet, 1.0 m/s	Adiabatic	Zero-gauge pressure	Adiabatic	30	20	20
	Fixed heat flux (1301.6 W)								
Case 4	Adiabatic		Pressure inlet, zero-gauge pressure						
	Fixed heat flux (950.1 W)								

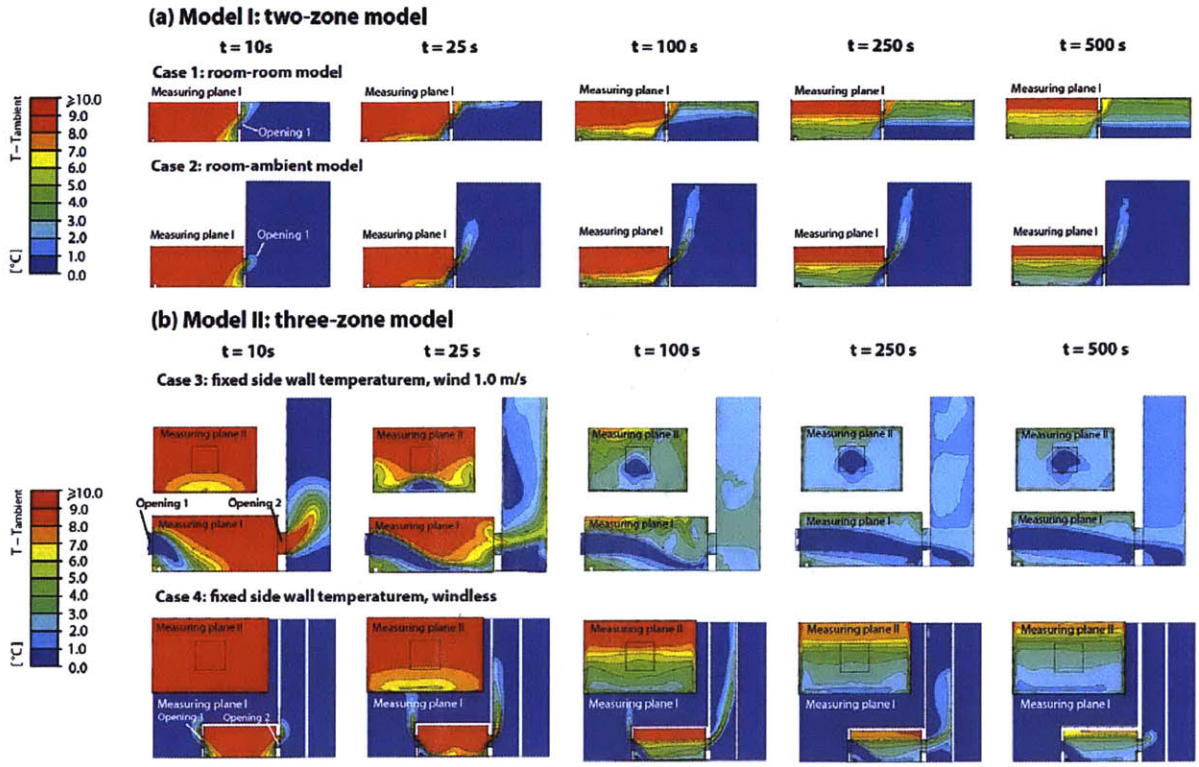

Figure 6-2. Temperature contours of Case 1, 2, 3 and 4 at t = 10 s, 25 s, 100 s, 250 s and 500 s from transient CFD simulation over 500 seconds. (a) cases 1 & 2; (b) cases 3 &4 .

6.3 Model development

6.3.1 Mass conservation

6.3.1.1 Flow network

We first satisfy the mass conservation criterion by understanding the flow network for the four cases from a global perspective, demonstrated in Figure 6-3. The arrows show the approximate flow directions observed in the CFD solutions.

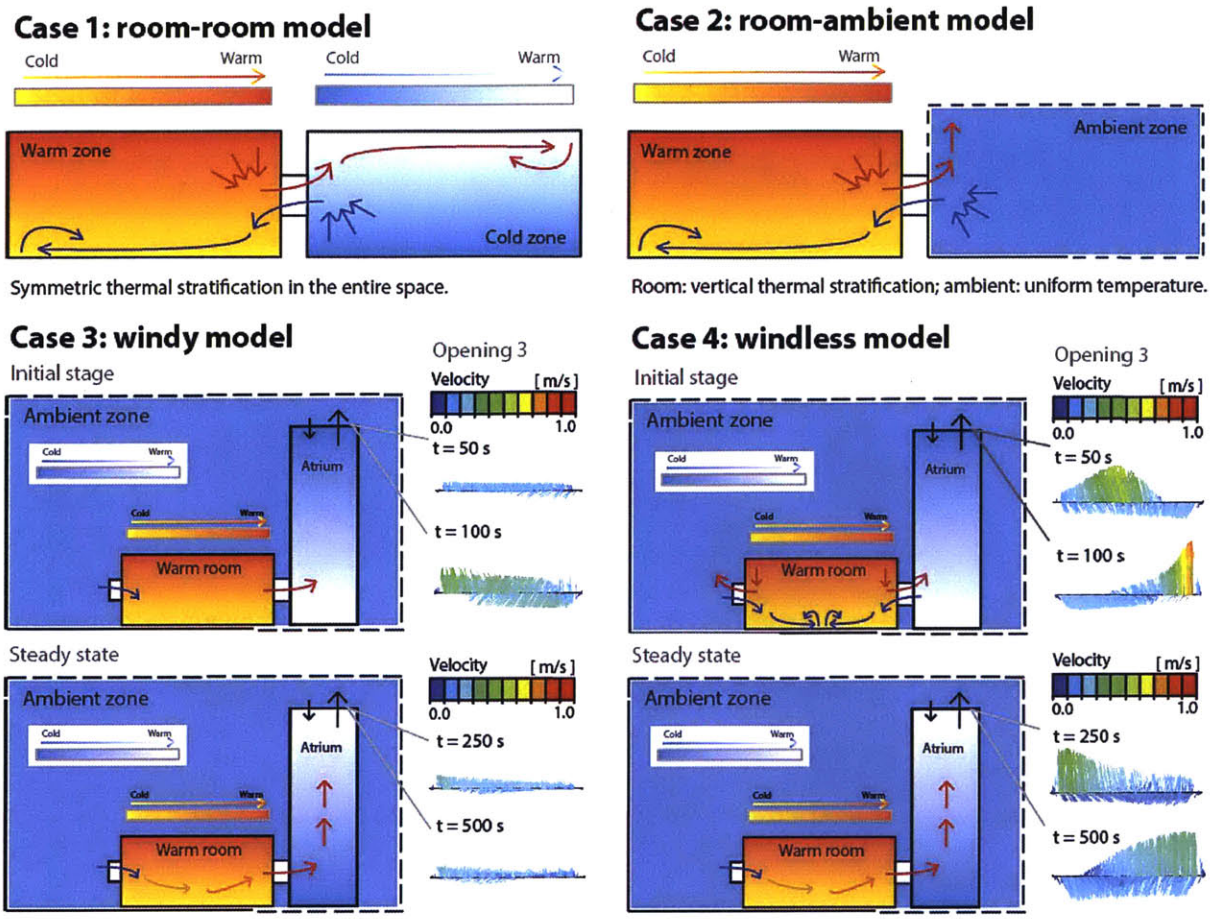

Figure 6-3. Schematic of the flow network in each of the four cases. For cases 3 and 4, the vector plots of the air velocity at entire opening 3 are extracted from the transient CFD simulations to present the backflow that we observed. The velocity plots at opening 3 are measured from cases 3(2) and 4(2).

For Case 1 & 2, it is assumed that the neutral plane is located at the middle height of the opening. For Case 3, the flow patterns at openings 1 and 2 are unidirectional yet there is bi-directional airflow at opening 3. This is mainly caused by flow oscillation and air entrainment from the ambient into the atrium at an unsteady flow rate. For Case 4, the flow network becomes more complicated in the presence of bi-directional airflow at all of the three openings including the atrium outlet. We thus satisfy mass conservation based on the flow network. For cases 1 & 2, the "natural convection model" relates mass flow rate to the stack pressure by assuming the

neutral plane is located right at the middle of the opening and introducing a discharge coefficient (C_d), as follows:

$$\text{Equation 6-1: } \dot{m} = \frac{1}{3} C_d \cdot A_{eff} \cdot \rho \cdot \sqrt{2 \frac{T_{warm} - T_{cold}}{T_{warm} + T_{cold}} \cdot g \cdot H}$$

where A_{eff} (m^2) is the effective opening area, which is the actual opening area (0.81 m^2) in the model; T_{warm} and T_{cold} (K) are the zonal averaged temperatures of the warm and cold zones; H (m) is the opening height.

For Case 3, mass conservation requires the net mass flow rate at each of the three openings to be the same, thus we have

$$\text{Equation 6-2: } \dot{m}_{net} = \dot{m}_1 = \dot{m}_2 = \dot{m}_{3+} - \dot{m}_{3-}$$

where $\dot{m}_1$ and $\dot{m}_2$ (kg/s) are the net mass flow rate at opening 1 and opening 2 (the flows are unidirectional), respectively; and $\dot{m}_{3+}$ and $\dot{m}_{3-}$ (kg/s) are the mass flow rate leaving and entering the atrium at opening 3.

For Case 4, bi-directional airflow is observed in all of the three openings, thus the mass conservation should be written as,

$$\text{Equation 6-3: } \dot{m}_{net} = \dot{m}_{1+} - \dot{m}_{1-} = \dot{m}_{2+} - \dot{m}_{2-} = \dot{m}_{3+} - \dot{m}_{3-}$$

where the signs indicate the flow directions at each opening: "+" means counterclockwise directions in the flow network while "-" means clockwise directions. Similarly, the mass flow rate can be calculated by total pressure difference by introducing a discharge coefficient for opening 1 in cases 3 and 4, for example.

Equation 6-4: $\dot{m}_{+} = C_d \rho w \int_{0.69}^{z_{NP}} \sqrt{2gz \cdot \frac{T_{warm} - T_{cold}}{T_{warm} + T_{cold}} + U^2} \cdot dz$

and $\dot{m}_{-} = C_d \rho w \int_{z_{NP}}^{1.59} \sqrt{2g(z - z_{NP}) \cdot \frac{T_{warm} - T_{cold}}{T_{warm} + T_{cold}} - U^2} \cdot dz$

where z_{NP} (m) is the neutral plane height, and U (m/s) is the freestream wind velocity, which is at 1.0 m/s in Case 3 and 0 in Case 4. The limits in the integral are the bottom height of the opening (0.69), neutral plane height Z_{NP}, and upper height of the opening (1.59). T_{warm} and T_{cold} are the warm and cold local temperatures.

6.3.1.2 Discharge coefficient

The discharge coefficient is an essential component in calculating the mass flow rate for each case. It is found to be largely dependent on the thermal conditions and geometric factors rather than being a constant, as is mentioned in chapter 2. However, for model simplicity, we assumes the discharge coefficient to be a constant although it is a function of temperature difference. This may cause some error and should be checked with caution for different situations.

6.3.1.3 Back flow rate

As previously mentioned, back flow pattern is observed at opening 3 for both cases 3 and 4 due to flow oscillation and air entrainment from the ambient into the atrium at an unsteady flow rate. A backflow rate, C_b, is defined as the mass ratio of the back flow from the ambient and the net flow through opening 3 that relates $\dot{m}_{3+}$ with $\dot{m}_{3-}$,

Equation 6-5: $C_b = \frac{m_{3-}}{m_{3+} - m_{3-}}$

For example, $C_b = 0$ means there is no ambient air flowing back into the atrium, while $C_b = 1$ means the back flow from the ambient is the same as the net flow. Figure 6-4 gives the calculated backflow rate for Cases 3 and 4 over 500 seconds from the CFD simulations. The results show that Case 3 have more fluctuations in the backflow rate than Case 4: in Case 3, the value of backflow rate vary drastically from 0 to 0.8; in Case 4, the coefficient increases quickly in the first 25 seconds and stabilizes at a high value (around 0.90). In general, the backflow rate is fluctuational owing to the thermal instability introduced by natural convection. The average backflow rate for each case

The back flow from the ambient cannot be neglected because the average backflow rate for each case is considerable (from 0.127 to 0.803), resulting in a large heat and mass transfer at opening 3. For Case 3, the presence of heat source plays a positive role in determining the backflow rate; the average backflow rate for with heat source is 0.370 whereas that for without heat source is 0.127. However, for Case 4, reach stable values quickly in the initial 50 seconds and the average values of the back flow rates are very close (roughly 0.80) regardless of the existence of heat sources. This disparity might be caused by the relatively high momentum of plumes in the windy cases that affects the entrainment from the ambient.

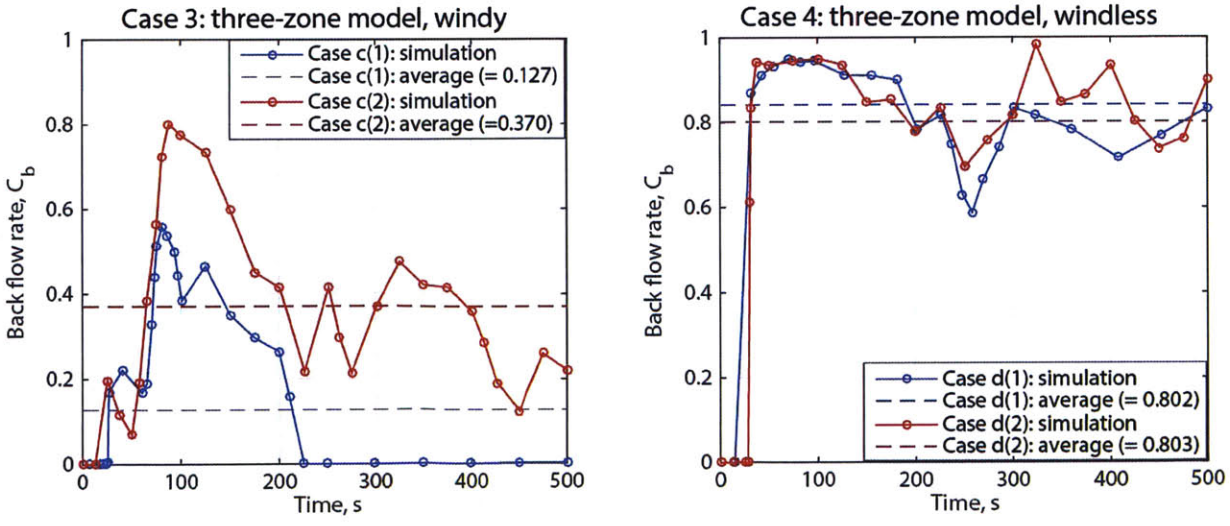

Figure 6-4. Back flow rate at opening 3 for cases 3 and 4 over 500 seconds.

6.3.2 Neutral plane

A key challenge is how to predict the neutral plane height so as to calculate the instantaneous bi-directional airflows in Case 4. We adopt the criteria of vertical pressure distributions using the well-mixed assumption (assumption 1). The vertical pressure gradient of each zone is simply $-\rho g$, where ρ is the density corresponding to the zonal averaged temperature. Therefore, we can plot the pressure distributions of each zone at different stages assuming no pressure drop at opening 3, as is shown in Figure 6-5. As previously mentioned, an interesting observation from the CFD is the transition from bi-directional airflow to unidirectional airflow. Initially, the ventilation is purely driven by local buoyancy forces and there is symmetric bi-directional flow pattern at both openings (Figure 6-5a). As the atrium gradually warms up, there establishes a pressure difference between the ambient and the atrium and the airflow pattern becomes unidirectional (Figure 6-5c). However, there is a phase where there is still bi-directional airflow pattern at opening 1, yet the airflow pattern at opening 2 has already become unidirectional (Figure 6-5b).

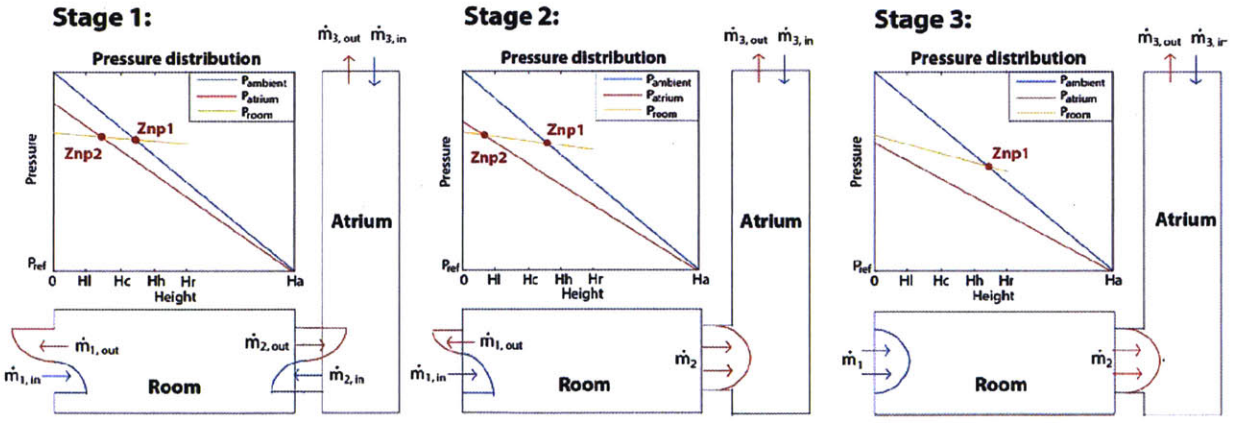

Figure 6-5. Schematic of the three ventilation stages in Case 4. The Z_{np1} and Z_{np2} are the neutral plane heights at openings 1 and 2, respectively.

In Figure 6-5, the Hl, Hc, and Hh are the bottom height, middle height, the upper height of the opening; $\dot{m}_{i,in}$ and $\dot{m}_{i,out}$ are the mass flow rates into and out of the next zone at the i^{th} opening.

We assume constant discharge coefficient for the openings so that the net mass flow rate at opening 1 can be calculated for demonstrative purposes:

Equation 6-6:
$$\begin{cases} \dot{m}_{1+} = C_d w \rho \int_{Z_{bot}}^{Z_{np1}} \sqrt{2\frac{P_{ambient} - P_{room}}{\rho}} dz = C_d w \int_{Z_{bot}}^{Z_{np1}} \sqrt{2\Delta\rho \cdot \rho g(Z_{np1} - z) + (\rho U)^2} dz \\ \dot{m}_{1-} = C_d w \rho \int_{Z_{np1}}^{Z_{top}} \sqrt{2\frac{P_{room} - P_{ambient}}{\rho}} dz = C_d w \int_{Z_{np1}}^{Z_{top}} \sqrt{2\Delta\rho \cdot \rho g(z - Z_{np1}) - (\rho U)^2} dz \end{cases}$$

To be noted, Equation 6-6 assumes that the wind pressure is not large enough to overwhelm the buoyancy forces so that there is still bi-directional flow. Nondimensionalization is then applied to the equations by introducing two non-dimensional groups:

Equation 6-7: $\bar{z} = \frac{z - z_{bot}}{H}$ and $\bar{\dot{m}} = \frac{\dot{m}}{C_d w \sqrt{2\Delta\rho \cdot \rho g H^3}}$ or $\bar{\dot{m}} = \frac{\dot{m}}{C_d w \rho \sqrt{2gH^3 \cdot \Delta T}}$

Thus the non-dimensional $\bar{\dot{m}}_+$, $\bar{\dot{m}}_-$ and $\bar{\dot{m}}_{net}$ between two zones of different thermal conditions (from warm zone to cold zone, or from cold zone to warm zone) can be calculated as follows:

Equation 6-8:
$$\begin{aligned} \bar{\dot{m}}_{net} &= \left| \int_0^{\bar{z}_{np}} \sqrt{(\bar{z}_{np} - \bar{z}) + \frac{\rho U^2}{2\Delta\rho \cdot gH}} d\bar{z} - \int_{\bar{z}_{np}}^1 \sqrt{(\bar{z} - \bar{z}_{np}) - \frac{\rho U^2}{2\Delta\rho \cdot gH}} d\bar{z} \right| \\ &= \frac{2}{3} \left| (\bar{z}_{np} + \frac{\rho U^2}{2\Delta\rho \cdot gH})^{\frac{3}{2}} - 2(\frac{\rho U^2}{2\Delta\rho \cdot gH})^{\frac{3}{2}} - [1 - (\bar{z}_{np} + \frac{\rho U^2}{2\Delta\rho \cdot gH})]^{\frac{3}{2}} \right| \end{aligned}$$

"Cold to warm":
$$\begin{cases} \bar{\dot{m}}_+ = \frac{2}{3} \left| (\bar{z}_{np} + \frac{\rho U^2}{2\Delta\rho \cdot gH})^{\frac{3}{2}} - 2(\frac{\rho U^2}{2\Delta\rho \cdot gH})^{\frac{3}{2}} \right| \\ \bar{\dot{m}}_- = \frac{2}{3} \left| [1 - (\bar{z}_{np} + \frac{\rho U^2}{2\Delta\rho \cdot gH})]^{\frac{3}{2}} \right| \end{cases}$$

or "warm to cold": $\begin{cases} \bar{\dot{m}}_{+} = \frac{2}{3}\left|[1-(\bar{z}_{np}+\frac{\rho U^2}{2\Delta\rho\cdot gH})]^{\frac{3}{2}}\right| \\ \bar{\dot{m}}_{-} = \frac{2}{3}\left|(\bar{z}_{np}+\frac{\rho U^2}{2\Delta\rho\cdot gH})^{\frac{3}{2}} - 2(\frac{\rho U^2}{2\Delta\rho\cdot gH})^{\frac{3}{2}}\right| \end{cases}$

The above equation contains the term of density difference and cannot be solved independently. However, if the ambient velocity is 0, then the dimensionless mass flow rates are purely functions of dimensionless neutral plane height. The equations can be written as,

Equation 6-9: $\bar{\dot{m}}_{net} = \left|\int_0^{\bar{z}_{np}} \sqrt{(\bar{z}_{np}-\bar{z})}d\bar{z} - \int_{\bar{z}_{np}}^1 \sqrt{(\bar{z}-\bar{z}_{np})}d\bar{z}\right| = \frac{2}{3}\left|\bar{z}_{np}^{\frac{3}{2}} - (1-\bar{z}_{np})^{\frac{3}{2}}\right|$

"Cold to warm": $\begin{cases} \bar{\dot{m}}_{+} = \frac{2}{3}\bar{z}_{np}^{3/2} \\ \bar{\dot{m}}_{-} = \frac{2}{3}\left|(1-\bar{z}_{np})^{\frac{3}{2}}\right| \end{cases}$ or "warm to cold": $\begin{cases} \bar{\dot{m}}_{+} = \frac{2}{3}\left|(1-\bar{z}_{np})^{\frac{3}{2}}\right| \\ \bar{\dot{m}}_{-} = \frac{2}{3}\left|(\bar{z}_{np})^{\frac{3}{2}}\right| \end{cases}$

Therefore, the above two equations relate the calculation of ventilation performance in each direction with the neutral plane height so that the coupling between ventilation and temperatures will be solved. It should also be noted that the above equations are universally applicable for the combined wind and buoyancy-driven natural ventilation since the above equations are based on nondimensionalization. Figure 6-6 gives the correlation between the dimensionless mass flow rate and the neutral plane height. It is interesting to notice that the net mass flow rate is approximately linearly correlated to nondimensional neutral plane height. The correlation between the dimensionless neutral plane height and the dimensionless mass flow rate is,

Equation 6-10: $\bar{\dot{m}}_{net} = 1.36\cdot\bar{z}_{NP} - 0.68$

Therefore, for one opening, we are able to use this correlation to linearly solve the coupling between the neutral plane height and the mass flow rate. That is to say, we automatically know

the nondimensional mass flow rate into and out of the each zone as soon as we know the neutral plane height location.

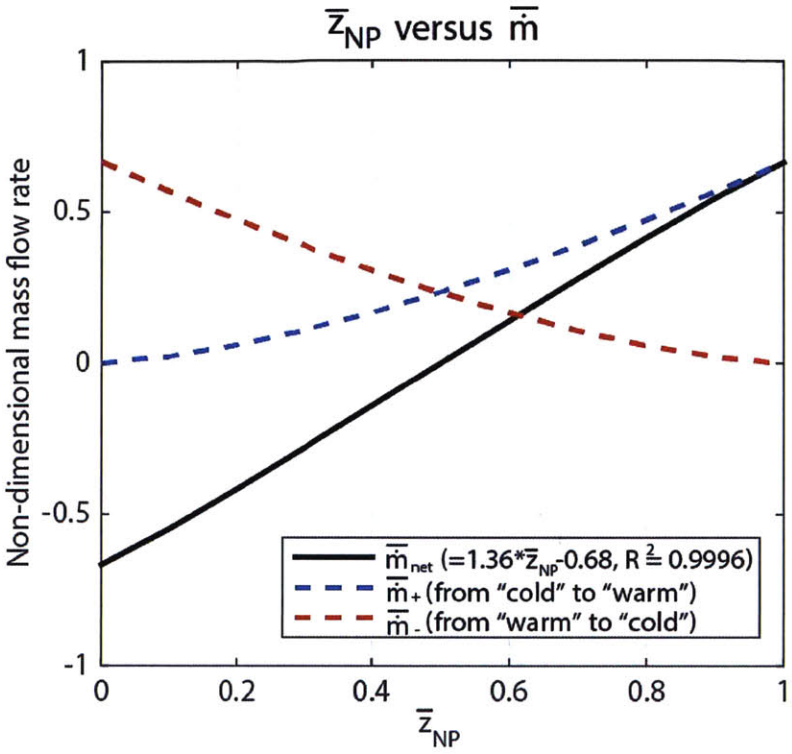

Figure 6-6. Implementation of the nondimensionalization for the neutral plane height and mass flow rate for the three zone model.

More importantly, the mass conservation requires the matching of flow rate between any of the three openings. We first satisfy the mass balance at openings 1 and 2. As is previously defined in the nondimensionalization, the mass flow rate of opening 1 and opening 2 can be calculated as,

Equation 6-11: $\dot{m}_{net1} = \bar{\dot{m}}_{net1} \cdot C_d w \sqrt{2\Delta\rho_1 \cdot \rho g H^3}$ and $\dot{m}_{net2} = \bar{\dot{m}}_{net2} \cdot C_d w \sqrt{2\Delta\rho_2 \cdot \rho g H^3}$

Mass conservation requires: $\dot{m}_{net1} = \dot{m}_{net2}$, therefore we have,

Equation 6-12: $\bar{\dot{m}}_{net1} \cdot \sqrt{T_{room} - T_{ambient}} = \bar{\dot{m}}_{net2} \cdot \sqrt{T_{room} - T_{atrium}}$.

This equation is derived at by assuming the height, width and discharge coefficient of the two openings are the same. In the equation, the T_{room}, $T_{ambient}$ and T_{atrium} are the local temperature of each zone, $\bar{\dot{m}}_{net1}$ and $\bar{\dot{m}}_{net2}$ are the net mass flow rates at openings 1 and 2. Using the linear correlation between the dimensionless neutral plane height and the net mass flow rate, shown in Figure 6-6, we can obtain:

Equation 6-13: $(1.36 \cdot \bar{z}_{NP1} - 0.68) \cdot \sqrt{T_{room} - T_{ambient}} = (0.68 - 1.36 \cdot \bar{z}_{NP2}) \cdot \sqrt{T_{room} - T_{atrium}}$.

Therefore, we can easily match the mass flow rates at openings 1 and 2 by setting the neutral plane height $\bar{z}_{NP2}$ at opening 2 at,

Equation 6-14: $\bar{z}_{NP2} = \frac{1}{2} - (\bar{z}_{NP1} - \frac{1}{2}) \cdot \sqrt{\frac{T_{room} - T_{ambient}}{T_{room} - T_{atrium}}}$.

As to opening 3, we only need to use the average value of the backflow rate measured from CFD simulations, shown in Figure 6-4, to calculate the inflow and outflow at opening 3. The inflow and out flow are:

Equation 6-15: $\dot{m}_{3+} = (1 + C_b) \cdot \dot{m}_{net}$ and $\dot{m}_{3-} = C_b \cdot \dot{m}_{net}$

6.3.3 Energy conservation

The previous section solves the coupling between the neutral plane height and mass flow rate, however, the location of the neutral plane height is changing over time and is coupled with the

energy conservation. Therefore, we make simplified assumptions to derive at the energy conservation for each case, they are:

- Assumption 1: the air in each zone is well-mixed such that each zone is a lumped body that contains homogeneous physical parameters (temperature, viscosity, density, etc.);
- Assumption 2: At each opening, for bi-directional flow between zone 1 and zone 2, the air flowing from zone 1 to zone 2 is of the temperature of zone 1, whereas the air flowing from zone 2 to zone 1 is of the temperature of zone 2; for unidirectional flow from zone 1 to zone 2, the air is of the zone 1 temperature;
- Assumption 3: The internal heat gain in each case is a constant throughout the entire process.

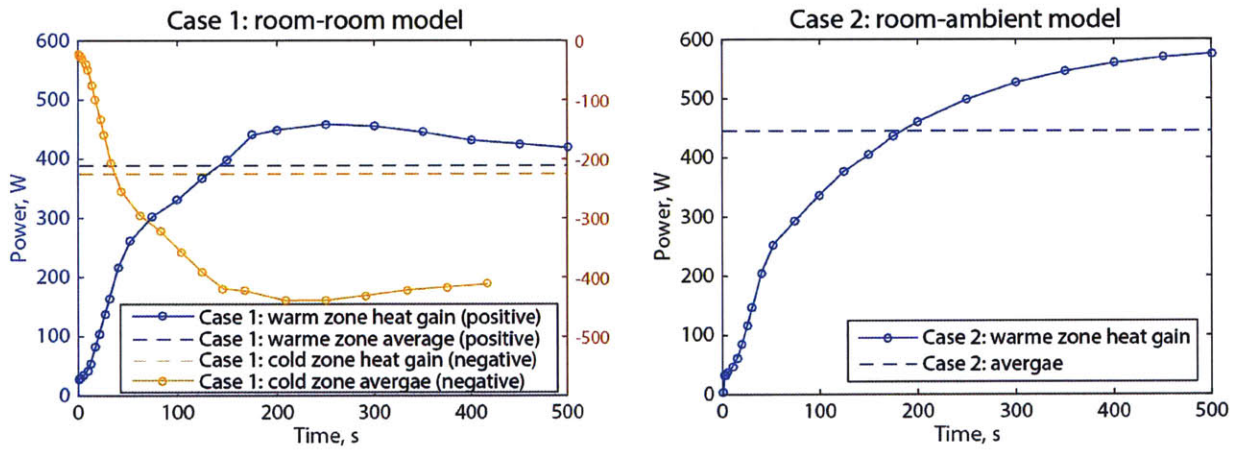

(a) (b)

Figure 6-7. Internal heat gains of two types of boundary conditions of cases 1 and 2 over 500 seconds.

Assumption 3 is an automatic assumption for the cases with constant heat flux in this chapter, but not true for the two zone model with fixed sidewall temperatures. To examine assumption 3 on internal heat gains, we measured the heat gains from the side walls for cases with fixed wall temperature for cases 1 and 2, as is shown in Figure 6-7.

The growth of heat flux in cases with fixed wall temperature boundary conditions increases within the first 200~300 seconds and then stabilizes at a relatively constant value. We use the averaged values (shown in Figure 6-7) of internal heat gains in our modeling framework for simplicity. However, when the internal heat gains vary drastically over the 500 seconds, this simplification might introduce important errors. Further investigations might be needed on approximating internal heat gains for different boundary conditions.

6.4 Numerical scheme

The internal heat gains, backflow rate and discharge coefficient are non-constant over time, however with limited information as well as for numerical simplicity, we might as well assume that those coefficients are constants. Therefore, we are able to arrive energy conservation for the four cases, shown in the control volume (C.V.) analysis below:

Equation 6-16:

Case 1:
$$\begin{cases} Warm \quad room: m_{warm} C_v \dfrac{\partial T_{warm}}{\partial t} = \dot{m} C_p (T_{cold} - T_{warm}) + HF_{warm} \\ Cold \quad room: m_{cold} C_v \dfrac{\partial T_{cold}}{\partial t} = \dot{m} C_p (T_{warm} - T_{cold}) + HF_{cold} \end{cases}$$

Case 2:
$$\begin{cases} Room: m_{room} C_v \dfrac{\partial T_{room}}{\partial t} = \dot{m} C_p (T_{ambient} - T_{room}) + HF_{room} \\ Ambient: T_{ambient} = 293.15K \end{cases}$$

Case 3:
$$\begin{cases} Room: m_{room} C_v \dfrac{\partial T_{room}}{\partial t} = \dot{m}_1 C_p (T_{ambient} - T_{room}) + HF_{warm} \\ Atrium: m_{atrium} C_v \dfrac{\partial T_{atrium}}{\partial t} = \dot{m}_2 C_p T_{room} - \dot{m}_{3+} C_p T_{atrium} + \dot{m}_{3-} C_p T_{ambient} \end{cases}$$

Case 4:
$$\begin{cases} Room: m_{room} C_v \dfrac{\partial T_{room}}{\partial t} = \dot{m}_{1+} C_p T_{ambient} + \dot{m}_{2-} C_p T_{atrium} - (\dot{m}_{1-} + \dot{m}_{2+}) C_p T_{room} + HF_{room} \\ Atrium: m_{atrium} C_v \dfrac{\partial T_{atrium}}{\partial t} = \dot{m}_{2+} C_p T_{room} + \dot{m}_{3-} C_p T_{ambient} - \dot{m}_{2-} C_p T_{atrium} - \dot{m}_{3+} C_p T_{atrium} \end{cases}$$

where T_{zone} is the zonal averaged temperature in each case, K; C_v and C_p are the specific heat capacities of the air, $J/(kg \cdot K)$; and HF is the internal heat gains through side walls, W; m_{zone} is the total mass of air in each zone, kg; and $\dot{m}$ is the mass flow rate at the opening, kg/s.

The model is based on the assumptions that the discharge coefficient, internal heat gains as well as the back flow rate can be approximated as constant. Therefore, the only challenge is to couple the temperature with mass flow rate. With the nondimensionalization we introduce in 6.3.2, it is possible to numerically solve the instantaneous neutral plane height, mass flow rate and temperatures by coupling the mass conservation and energy conservation simultaneously based on the assumptions made before. More precisely, the numerical scheme will contain three steps:

1) Calculate the 1st time step neutral plane height at both openings, $Z_{np1}(t_1)$ and $Z_{np2}(t_1)$, as well as zonal temperature of each zone $T_{room}(t_1)$, $T_{atrium}(t_1)$ and $T_{ambient}(t_1)$. The initial neutral plane height at opening 1 is defined by initial condition, $Z_{np2}(t_1)$ can be calculated using nondimensionalization introduced in Equation 6-14. The 1st time step mass flow rate at each opening can be calculated by Equations 6-10 and 6-7.

2) Use the control volume analysis and the 1st time step parameters including the mass flowrate (inflows and outflows), temperature of each zone to calculate the 2nd time step temperatures of the room and atrium, $T_{room}(t_2)$ and $T_{atrium}(t_2)$.

3) As the atrium temperature warms up, the neutral plane height is also moving. We make a critical assumption that

Equation 6-17: $$\overline{z}_{NP1}(t_2) = (\frac{1}{2} - \overline{z}_{NP2}(t_1)) \cdot \sqrt{\frac{T_{room}(t_2) - T_{atrium}(t_2)}{T_{room}(t_2) - T_{ambient}(t_2)}} + \frac{1}{2}$$

And then the neutral plane height at opening 2 can be calculated using Equation 6-14. Then repeat steps 2 and 3 for the following time steps.

6.5 Conclusions

We demonstrate a multi-physics modelling framework for fast prediction of bi-directional natural ventilation, which still needs validation with CFD and experimental results. The model couples the instantaneous thermal and ventilation performances as well as neutral plane height by mass, energy and momentum conservations. It provides insights into the role of bi-directional flow in determining the final state ventilation and thermal performances and offers important fast prediction tools for design purposes. This model may provide a deep understanding of the unsolved questions on the neutral plane height for buoyancy-driven flows in buildings with multiple openings. The approximation derived from nondimensionalization can be extended to more universal building settings but the complexity of the flow network can result in multiple solutions and system instability, which needs further considerations and investigations. Considerations might also be needed to investigate whether the assumptions are valid that the discharge coefficient, heat gains, and backflow rate can be treated as constants.

7. CONCLUSIONS AND OUTLOOK

7.1 Conclusions

In general, this thesis can be divided into two parts. Part 1 is about single-sided bi-directional buoyancy-driven natural ventilation; part 2 is about multi-zone bi-directional natural ventilation under assisting wind and buoyancy forces.

For single-sided buoyancy ventilation, this thesis investigate the role of thermal stratifications on the discharge coefficient and propose a reasonable explanation for the controversy in the coefficient through extensive CFD simulations. We propose that the single-sided buoyancy-driven ventilation is mainly dominated by local thermal and geometric conditions, and that different thermal stratification patterns will result in deviations between the local temperature difference and the zonal temperature difference. Therefore, the traditional discharge coefficient as defined by the zonal temperature difference is unable to accurately reflect the local thermal conditions, leading to its widely varying nature. A new concept of the local discharge coefficient that is defined by the local temperature difference near the opening region. It is shown by CFD that the local discharge coefficient shows better consistency under various thermal stratification patterns for both room-room and room-ambient scenarios. It is considered to be a better gauge for estimating single-sided ventilation because it is able to rule out the influence of thermal stratifications, especially for buildings with localized heat sources.

Moreover, we investigate the influence of accounting for radiative heat exchange and neglecting it on the air flow and thermal dynamics of a space ventilated using buoyancy-driven flow. It is found that ignoring the effects of radiation can cause a consistent underestimation of the mass flowrate for the two-way flow model. Neglecting radiation results in an unrealistic thermal stratification profiles, especially when the heat source is concentrated in a small region. Scale water models might be useful when analyzing cases with distributed heat sources or with an opening in the middle of the height of the room. Nevertheless, even in these situation, it should be considered that in the real-sized space, the temperature of the air surrounding the occupants

might be approximately 2 °C higher and the mass flowrate 16% higher than in the scale water model. Consequently, temperature profiles, mass flowrates, surface temperatures and any other results that depend on these variables are of limited usefulness in realistic spaces, when obtained using computational or experimental methods that ignore the effects of radiation.

For the multi-zone model, we visualize the flow development for the cases with and without wind. In the windless cases with a moderate to high wind velocity, the CFD simulations suggest that bi-directional flow occurs during the initial stage at both openings 1 and 2 that warms up the atrium and causes a pressure difference between the ambient and the atrium, resulting in unidirectional flow at steady states. In the windy cases, the flow pattern in the CFD simulations throughout the whole process was unidirectional because the initial net flow is non-zero in the presence of wind pressure. The results suggest that initial bi-directional flow pattern will affect the steady state solutions; neglecting bi-directional flow in natural ventilation will result in inaccurate estimations and problematic solutions of natural ventilation, casting doubt to the unidirectional flow assumption that is often made in conventional flow network models.

A multi-physics modelling framework is developed for fast prediction of bi-directional natural ventilation, which still needs validation with CFD and experimental results. The model is able to predict the instantaneous thermal and ventilation performances as well as neutral plane height and capture the transitional airflow pattern by mass, energy and momentum conservations. It provides insights into the role of bi-directional flow in determining the final state ventilation and thermal performances and offers important fast prediction tools for design purposes.

7.2 Limitations and outlook

There are a few limitations in this work, listed as follows:

1) The local discharge coefficient is still a function of temperature difference as well as geometric factors; more investigation is needed for thorough understanding. This suggests that using the typical value of 0.62 for the discharge coefficient might result in large errors in estimating the ventilation performance in single-sided ventilation. It is also observed that the discharge coefficients for FWT and FHF cases in the room-ambient model are relatively more stable than in the room-room scenario regardless of the change of opening geometry and temperature difference. This might be attributed to the fact that the ambient zone is at a uniform temperature, as well as the fact that there is less geometric restriction in the ambient zone.

2) Although the concept of local discharge coefficient is shown to be able to rule out the influence of thermal stratifications, it is difficult to be implemented. It is easier to use the zonal averaged temperature difference because it reflects the bulk property. The challenge is how to relate the zonal temperature difference to local temperature difference. The correlation should be different for different thermal stratifications/boundary conditions. Meanwhile, we define the local temperature difference as the temperature difference between the cuboid regions that are within 1.0 m distant across the opening height. This definition may need to be re-considered when the heater is located near the opening.

3) The model for predicting the transient flow behaviors as well as thermal conditions may provide a deep understanding of the unsolved questions on the neutral plane height for buoyancy-driven flows in buildings with multiple openings. The approximation derived from nondimensionalization can be extended to more universal building settings but the complexity of the flow network can result in multiple solutions and system instability, which needs further considerations and investigations. Considerations might also be needed to investigate whether the assumptions are valid that the discharge coefficient, heat gains, and backflow rate can be treated as constants.

4) The geometry that we consider for the multi-zone natural ventilation is a simple scenario. There are more cases where bi-directional flow is important in determining the steady state solutions. Those cases need to be fully generalized and taken into consideration as well.

Therefore, more effort should be put into understanding the bi-directional natural ventilation and developing useful tools for fast predicting the bi-directional natural ventilation. Simplified methods can be developed to reduce the calculation complexity. The bi-directional flow pattern might be able to answer many unsolved questions on multiple as well as inaccurate solution, leading to more accurate and faster simulation tools for natural ventilation design and assessment.

On the other hand, more attention should be paid to the bi-directional flow as well as natural ventilation in general through openings with complex geometries such as commercial windows and doors. It is more common in real buildings than ventilation through plain rectangular openings yet very limited investigations have been made on the flow through complex openings. As the opening geometry becomes more complex, the ventilation through openings can be three dimensional and new challenges may come out for understanding the flow characteristics.

REFERENCE

Chapter 1

[1] Buildings Energy Databook, 2011. US Department of Energy and Annual Energy Review (2012). Energy Information Administration, U.S. Department of Energy. March 2012. http://buildingsdatabook.eren.doe.gov/DataBooks.aspx.

[2] Perez-Lombard, L. Ortiz, J. and Pout, C. 2008. "A review on buildings energy consumption information." *Energy and Buildings* 40(3), 394-398.

[3] Batterman, S. A. and Burge, H. 1995. "HVAC systems as emission source affecting indoor air quality: a critical review." *HVAC&R Research* 1(1), 61-78.

[4] Bearg, D. W. 1993. "Indoor Air Quality and HVAC Systems." Chelsea, Mich: Lewis Publishers.

[5] Brager, G. S. de Dear, R. 2000. "A standard for natural ventilation." *ASHRAE Journal* 42(10), 21-28.

[6] Fehrenbacher, J. 2008. "RUSSIA TOWER – World's largest naturally ventilated building." http://inhabitat.com/russia-tower-worlds-largest-naturally-ventilated-building/

[7] Allocca, C. Chen, Q and Glicksman L. R. 2003. "Design analysis of single-sided natural ventialtion." *Energy and Buildings* 35(8), 785-795.

[8] Sundell, J. 2004. "On the history of indoor air quality and health." *Indoor Air* 14(7), 51-58.

[9] de Dear, R. and Brager, G. 2002. "Thermal comfort in naturally ventilated buildings: revision to ASHRAE Standard 55." *Energy and Buildings* 34(6), 549-561.

[10] Allard, F. Natural Ventilation in Buildings: A Design Handbook, James & James Ltd., London, 1998.

[11] Stavrakakis, G. M., Koukou, M. K. and etc. 2008. "Natural cross-ventilation in buildings: Building-scale experiments, numerical simulations and thermal comfort evaluations." *Energy and Buildings* 40(9), 1666-1681.

[12] Riffat, S. B. 1989. "Measurement of heat and mass transfer between the lower and upper floors of a house." *Int. J. Energy Research* 3, 231-241.

[13] Favarolo, P. A. and Manz, H. 2005. "Temperature-driven single-sided ventilation through a

large rectangular opening." *Building and Environment* 40(5), 689-699/

[14] Brown, W. G. and Solvason, K. R. 1962. "Natural convection through rectangular openings in partitions – 1: Vertical partitions." *International Journal of Heat and Mass Transfer* 5(9), 863-862-868.

[15] Bolster, D. Mailard, A. and Linden, P. 2008. "The response of natural displacement ventilation in time-varying heat sources." *Energy and Buildings* 40(12), 2099-2110.

[16] Hunt, G. R. and Linden, P. F. 1998. "Time-dependent displacement ventilation caused by variations in internal heat gains: Application to a lecture theatre." *International Conference on Air Distribution in rooms*, Stockholm, SUEDE.

[17] Emswiler, J. E. and Randall W. C. 1926. "The neutral zone in ventilation". *Engineering Research Bulletin* No. 3.

[18] Brown, W. G. Wilson, A. G. and Solvason, K. R. 1963. "Heat and Moisture Flow Through Openings by Convection," *ASHRAE Journal* 5(9), 49-54.

[19] Shaw, B. H. 1976. "Heat and mass transfer by convection through large rectangular openings in vertical partitions." Doctoral thesis, University of Glasgow.

[20] Shaw, B. H. Whyte, W. 1974. "Air movement through doorways: the influence of temperature and its control by forced air flow", *Building Service Engeering* 42, 210-218.

[21] Barakat, S. A. 1978. "Inter-zone convective heat transfer in buildings: a review." *Journal of Solar Energy Engineering* 109, 71-78.

[22] Riffat, S. B. 1989. "Measurement of heat and mass transfer between the lower and upper floors of a house." *International Journal of Energy Research* 3, 231-241.

[23] Wilson, D. J. Kiel, D. E. 1990. "Gravity driven counter-flow through an open door in a sealed room." *Building and Environment* 25(4), 379-388.

[24] Jiang, Yi. Chen, Qingyan. 2003. "Buoyancy-driven single-sided natural ventilation in buildings with large openings." *International Journal of Heat and Mass Transfer* 46, 973-988.

[25] von Grabe, J. 2013. "Flow resistance for different types of windows in the case of buoyancy ventilation." *Energy and Buildings* 65, 516-522.

[26] von Grabe, J. Svoboda, P. Baumler, A. 2014. "Window ventilation efficiency in the case of buoyancy ventilation." *Energy and Buildings* 72, 203-211.

[27] Li, Y. Delsante, A. "On natural ventilation of a building with two openings." Procedding 19th AIVC Conference on Ventilation Technologies in Urban Areas, Oslo, Norway, 28–30 September, 1998.

[28] Li, Y. Delsante, A. 2001. "Natural ventilation induced by combined wind and thermal forces." *Building and Environment* 36, 59–71.

[29] Gladstone, C. Woods, A. W. 2001. "On buoyancy-driven natural ventilation of a room with a heated floor." *Journal of Fluid Mechanics* 441, 293–314.

[30] Heiselberg, P. Li, Y. Andersen, A. Bjerre, and M. Chen, Z. 2004. "Experimental and CFD Investigation of dynamical phenomena in a naturally ventilated building." *Indoor Air* 14, 43–54.

[31] Yuan, J. Glicksman L. R. 2008. "Multiple steady states in combined buoyancy and wind driven natural ventilation: The conditions for multiple solutions and the critical point for initial conditions." *Building and Environment* 43(1), 62-69.

[32] Duan, S. Li, Y. 2005. "An example of solution multiplicity in a building with bi-directional flow openings." *Indoor and Built Environment* 14(5), 359-369.

Chapter 2

[1] Larsen, T. S. Heiselberg, P. 2008. "Single-sided natural ventilation driven by wind and temperature difference." *Energy and Buildings* 40, 1031-1040.

[2] Warren, P.R. Parkins, L.M. 1985. "Single-sided ventilation through open windows." Conference Proceedings, Thermal Performance of the Exterior Envelopes of Buildings, Florida, ASHRAE SP 49, 209–228.

[3] Katsumichi, N. 2003. "Ventilation calculation by network model inducing bi-directional flows in openings." Eighth International IBPSA Conference. Eindhoven, Netherlands, Aug 11-14.

Chapter 3

[1] Brager, G.S. and de Dear, R. J. 2000. "A standard for natural ventilation." *ASHRAE Journal*

42.10(21). Sundell, J. 2004. "On the history of indoor air quality and health". *Indoor Air* 14(s7), 51-58.

[2] de Dear, R. and Brager, G.S. 2002. "Thermal comfort in naturally ventilated buildings: revisions to ASHRAE Standard 55." *Energy and Buildings* 34(6), 549–561.

[3] Linden, P. F. 1999. "The fluid mechanics in natural ventilation." *Annual Review of Fluid Mechanics* 31, 201-238.

[4] Allocca, C. Chen, Q. and Glicksman, L. R. 2003. "Design analysis of single-sided natural ventilation". *Energy and Buildings* 35(8), 785-795.

[5] Santamouris, M. and Allard, F. 1998. "Natural ventilation in buildings: a design handbook". Published by James & James L.td, UK.

[6] Emswiler, J. E. and Randall W. C. 1926. "The neutral zone in ventilation". *Engineering Research Bulletin* No. 3.

[7] Brown, W. G. and Solvason, K. R. 1962. "Natural convection through rectangular openings in partitions – 1: Vertical partitions." *International Journal of Heat and Mass Transfer* 5(9), 863-862-868.

[8] Shaw, B. H. 1971. "Heat and mass transfer by natural convection and combined natural and forced air flow through large rectangular openings in a vertical partition." *Symposium on Heat and Mass Transfer by Combined Forced and Natural Convection*, IMechE, Sept. 15, Paper No. CI 17/71.

[9] Barakat, S. A. 1978. "Inter-zone convective heat transfer in buildings: a review." *J. Solar Energy Engineering* 109, 71-78.

[10] Riffat, S. B. 1989. "Measurement of heat and mass transfer between the lower and upper floors of a house." *Int. J. Energy Research* 3, 231-241.

[11] Wilson D. J. and Kiel D. E. 1990. "Gravity driven counter-flow through an open door in a sealed room." *Building and Environment*, 25(4), 379-388.

[12] Jiang, Y. Chen, Q. 2003. "Buoyancy-driven single-sided natural ventilation in buildings with large openings." *Int. J. Heat Mass Transfer* 46, 973-988.

[13] Chen, Q. 1995. "Comparison of different k-ε models for indoor air flow computations." *Numerical heat transfer. Part B, Fundamentals*, 28(3), 353-369.

[14] Leckner, B. 1972. "Spectral and total emissivity of water vapor and carbon dioxide."

Combustion and flame 19(1), 33–48.

[15] Favarolo, P. A. Manz, H. 2005. "Temperature-driven single-sided ventilation through a large rectangular opening." *Building and Environment* 40(5), 689-699.

Chapter 4

[1] Linden, P. F. Lane-Serff, G. F. and Smeed, D. A. 1990. "Emptying filling boxes: the fluid mechanics of natural ventilation." *Journal of Fluid Mechanics* 212, 309–335.

[2] Hunt, G. R. Linden, P. F. 1999. "The fluid mechanics of natural ventilation – displacement ventilation by buoyancy-driven flows assisted by wind." *Building and Environment* 34(6), 707-720.

[3] Gladstone, C. Woods, A. W. 2001. "On buoyancy-driven natural ventilation of a room with a heated floor." *Journal of Fluid Mechanics* 441, 293-314.

[4] Mundt, E. 1996. "The performance of displacement ventilation systems: experimental and theoretical studies." *Kungliga Tekniska Hogskolan: Sweden.*

[5] Menchaca-Brandan, M.A. 2012. "Study of Airflow and Thermal Stratification in Naturally Ventilated Rooms." *PhD thesis, Massachusetts Institute of Technology.*

[6] Menchaca-Brandan, M. and Glicksman L. R. 2011. "The importance of accounting for radiative heat transfer in room airflow simulations." *Proceedings of ROOMVENT 2011 Conference, Trondheim, Norway.*

Chapter 5

[1] Larsen, T. S. Heiselberg, P. 2008. "Single-sided natural ventilation driven by wind and temperature difference." *Energy and Buildings* 40, 1031-1040.

[2] Etheridge, D. W. 2000. "Unsteady flow effects due to fluctuating wind pressures in natural ventilation design—instantaneous flow rates." *Building and Environment* 35(4), 321-337.

[3] van Hooff, T. Blocken, B. "On the effect of wind direction and urban surroundings on natural

ventilation of a large semi-enclosed stadium." *Computers and Fluids* 39(7), 1146-1155.

[4] Linden, P. F. 1999. "The fluid mechanics in natural ventilation." *Annual Review of Fluid Mechanics* 31, 201-238.

[5] Holford, J. M. and Hunt, G. R. 2003. "Fundamental atrium design for natural ventilation." *Building and Environment* 38(3), 409-426.

[6] Allocca, C. Chen, Q. and Glicksman, L. R. 2003. "Design analysis of single-sided natural ventilation". *Energy and Buildings* 35(8), 785-795.

[7] Andersen, K. T. 2003. "Theory for natural ventilation by thermal buoyancy in one zone with uniform temperature." *Building and Environment* 38(11), 1281-1289.

[8] Emswiler, J. E. and Randall W. C. 1926. "The neutral zone in ventilation". *Engineering Research Bulletin* No. 3.

[9] Li, Y. and Delsante, A. 1998. "On natural ventilation of a building with two openings." *Proceeding 19th of AIVC Conference on Ventilation Technologies in Urban Areas*, Oslo, Norway, 28-30 September 1998.

[10] Gladstone, C. Woods, A. W. 2001. "On buoyancy-driven natural ventilation of a room with a heated floor." *Journal of Fluid Mechanics* 441, 293–314.

[11] Duan, S. Li, Y. 2005. "An example of solution multiplicity in a building with bi-directional flow openings." *Indoor and Built Environment* 14(5), 359-369.

[12] Hunt, G. R. and Linden, P. F. 1998. "Time-dependent displacement ventilation caused by variations in internal heat gains: Application to a lecture theatre." *International Conference on Air Distribution in rooms*, Stockholm, SUEDE.

[13] Jiang, Yi. Chen, Qingyan. 2003. "Buoyancy-driven single-sided natural ventilation in buildings with large openings." *International Journal of Heat and Mass Transfer* 46, 973-988.

[14] Chen, Q. 1995. "Comparison of different k-ε models for indoor air flow computations." *Numerical heat transfer. Part B, Fundamentals*, 28(3), 353-369.

[15] Glicksman, L.R. and Chen, Q. 1998. "Interaction of Radiation Absorbed by Moisture in Air with Other Forms of Heat Transfer in Enclosure." *Proceedings of ROOMVENT '98 Con*ference 2, 111-118, Stockholm, Sweden.

[16] Leckner, B. 1972. "Spectral and total emissivity of water vapor and carbon dioxide."

Combustion and flame 19(1), 33–48.

[17] Avdelidis, N. P. and Moropoulou, A. 2003. "Emissivity considerations in building thermography." *Energy and Buildings* 35(7), 663-667.

[18] Nansteel, M. W. and Greif, R. 1981. "Natural convection in undivided and partially divided rectangular enclosures." *Journal of Heat Transfer* 103, 623.

[19] Olson, D. A. Glicksman, L. R. and Ferm, H. M. 1990. "Steady-state natural convection in empty and partitioned enclosures at high Rayleigh numbers." *Journal of Heat Transfer* (Transactions of the ASME (American Society of Mechanical Engineers), Series C), 112 (3).

[20] Menchaca, A. and Glicksman, L. 2008. "CoolVent: a multizone airflow and thermal analysis simulator for natural ventilation in buildings." *Third national conference of IBPSA-USA*, Berkeley, California, July 30 – Aug 1, 2008.

Chapter 6

[1] Hunt, G. R. and Linden, P. F. 1998. "Time-dependent displacement ventilation caused by variations in internal heat gains: Application to a lecture theatre." *International Conference on Air Distribution in rooms*, Stockholm, SUEDE.

[2] Duan, S. Li, Y. 2005. "An example of solution multiplicity in a building with bi-directional flow openings." *Indoor and Built Environment* 14(5), 359-369.

[3] Shafiee, S. Topal, E. 2008. "When will fossil fuel reserves be diminished?" *Energy Policy* 37(1), 181-189.

[4] Withagen, C. 1994. "Pollution and exhaustibility of fossil fuels." *Resource and Energy Economics* 16(3), 235-242.

[5] Stern, N. 2007. "The Economics of Climate Change." Cambridge Univ. Press, Cambridge.

[6] Brager, G.S. and de Dear, R. J. 2000. "A standard for natural ventilation." *ASHRAE Journal* 42.10(21). Sundell, J. 2004. "On the history of indoor air quality and health". *Indoor Air* 14(s7), 51-58.

[7] Bearg, D. W. 1993. "Indoor Air Quality and HVAC Systems." Chelsea, Mich: Lewis

Publishers.

[8] de Dear, R. and Brager, G.S. 2002. "Thermal comfort in naturally ventilated buildings: revisions to ASHRAE Standard 55." *Energy and Buildings* 34(6), 549–561.

[9] Emswiler, J. E. and Randall W. C. 1926. "The neutral zone in ventilation". *Engineering Research Bulletin* No. 3.

[10] Hunt, G. R. and Linden, P. F. 1998. "Time-dependent displacement ventilation caused by variations in internal heat gains: Application to a lecture theatre." *International Conference on Air Distribution in rooms*, Stockholm, SUEDE.